

Distinguishing Artificial and Essential Symmetry Breaking in a Single Determinant: Approach and Application to the C_{60} , C_{36} , and C_{20} Fullerenes

Joonho Lee* and Martin Head-Gordon*

*Department of Chemistry, University of California, Berkeley, California 94720, USA
Chemical Sciences Division, Lawrence Berkeley National Laboratory, Berkeley, California
94720, USA*

E-mail: linusjoonho@gmail.com; mhg@cchem.berkeley.edu

Abstract

We present a thorough analysis of symmetry breaking observed in Hartree-Fock (HF) solutions of fullerenes C_{60} , C_{36} , and C_{20} in order to characterize the nature of electron correlation in them. Our analysis is based on (1) the critical regularization strength to restore symmetry breaking in the recently developed regularized orbital optimized second-order Møller-Plesset perturbation theory (κ -OOMP2), (2) singlet-triplet gaps from various MP2 methods, and (3) natural orbital occupation numbers from restricted coupled-cluster with singles and doubles (RCCSD) and coupled-cluster valence bond with singles and doubles (CCVB-SD). Based on these three independent probes, we conclude that C_{36} (D_{6h}) exhibits genuine strong correlation and symmetry breaking whereas C_{60} exhibits *artificial* HF symmetry breaking and is not strongly correlated. Investigating the critical regularization strength, we discuss strong correlation in C_{20} at the Jahn-Teller distorted geometries (C_{2h} , D_{2h} , C_i , and D_{3h}) and the I_h geometry. Only C_{20} (I_h) was found to be strongly correlated while others exhibit *artificial* HF symmetry breaking. This analysis highlights a useful feature of the recommended κ -OOMP2 method. It is an electronic structure method that describes dynamic correlation, and attenuates strong correlation in MP2 towards zero by regularization. Therefore, κ -OOMP2 will exhibit symmetry breaking in its reference determinant only when correlation is strong (i.e., essential symmetry breaking). Artificial symmetry breaking (arising in HF due to neglect of dynamic correlation) is thus removed in κ -OOMP2.

1 Introduction

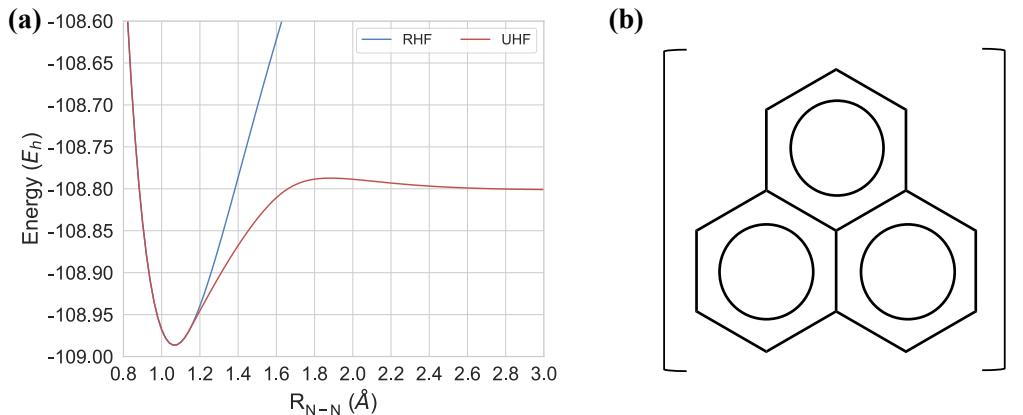


Figure 1: (a) Bond dissociation of N_2 in the cc-pVTZ basis set and (b) a phenalenyl radical. In (a), RHF stands for spin-restricted Hartree-Fock and UHF stands for spin-unrestricted Hartree-Fock. The Coulson-Fischer point is located at 1.16 Å.

The conventional wisdom in quantum chemistry is that spin symmetry-breaking is often necessary for describing strongly correlated systems that are beyond the scope of single-reference wavefunctions with spin-restricted orbitals.^{1,2} A familiar example, illustrated in Figure 1 (a) is the spin-polarization that occurs in homolytic bond-breaking at the Coulson-Fischer point,³ leading to spin-unrestricted fragments at separation. We can say that this is *essential symmetry-breaking*, because without it, the character of a one-determinant wavefunction is fundamentally wrong (it has ionic character at dissociation). This is analogous to the fact that the exact wavefunction in this recoupling regime has *essential* multiconfigurational character, and is not qualitatively similar to a single determinant of spin-restricted orbitals. In other words, essential symmetry-breaking yields qualitatively better energies because it captures some aspects of electron correlation relative to a spin-restricted determinant.

However, *artificial symmetry breaking* has appeared in numerous systems including open-shell systems and polycyclic aromatic hydrocarbons.⁴⁻¹¹ It is “artificial” in the sense that these systems are not strongly correlated and a single Slater determinant wavefunction with restricted orbitals should be a faithful representation. However, employing unrestricted Hartree-Fock

(UHF) wavefunctions often yields significantly spin-contaminated results, which then generally give poor energetics. An example is the doublet phenalenyl radical, shown in Figure 1 (b), which is quite stable, with known solution chemistry.^{12,13} Yet UHF/6-31G* calculations lead to $\langle \hat{S}^2 \rangle = 2.08$ rather than 0.75,¹⁴ even though there is no obvious “essential” electron correlation effect that is captured by this extensive spin symmetry-breaking. Rather we might say that this “artificial” symmetry-breaking is lowering the energy by recovering a bit of the dynamical correlation.

It is another difficult *symmetry dilemma* as to how to distinguish a genuine symmetry breaking from an artificial one.¹⁵ At the mean-field level, spontaneous symmetry breaking occurs to lower the mean-field electronic energy. Broken symmetry solutions are variationally preferred due to the very limited form of a single determinant wavefunction. However, subsequent correlated wavefunction calculations (particularly those that include perturbative corrections) on top of broken symmetry orbitals often yield qualitatively incorrect energetics and properties.^{6,7,10,16–20}

To mitigate this problem, it is often preferred to employ approximate Brückner orbitals.^{21–24} The exact Brückner orbitals may be obtained from an exact wavefunction by enforcing the zero singles constraint (i.e. the defining property of Brückner orbitals).^{25,26} Having an exact wavefunction is not a realistic assumption so, in practice, one may utilize coupled-cluster doubles (CCD) to obtain so-called Brückner doubles (BD).²⁴ Our group proposed a variational formulation of BD, called orbital-optimized doubles (OD), which optimizes orbitals in the presence of the CCD correlation energy.^{27,28}

One major drawback of OD (or BD) is that its computational complexity scales sextically with system size. A more economical way to obtain approximate Brückner orbitals with fifth-order complexity is to use orbital-optimized second-order Møller-Plesset theory (OOMP2).¹⁴ OOMP2 has been successfully applied to shed light on artificial spin-symmetry breaking problems.^{29,30} It also improves energetics of radical-involving systems drastically compared to regular MP2.^{31,32}

Although OOMP2 has shown its utility in the aforementioned examples, it also has two disturbing features.^{33,34} First, its potential energy surface often exhibits a first-order derivative discontinuity even though the electronic energy is minimized with respect to orbitals which should give only a second-order derivative discontinuity. This is a consequence of the disappearance of Coulson-Fischer points.³ Second, it often finds a divergent energy solution (i.e. $E = -\infty$) by preferring a unphysical zero-gap restricted solution. We argue that these two drawbacks were satisfactorily solved and thoroughly analyzed in our previous work where we employed an orbital energy dependent regularizer.³⁵

Fullerenes have attracted great attention in physical chemistry and interested readers are referred to ref. 36, an excellent textbook which summarizes the history of fullerenes in physical chemistry, and references therein. Starting from the smallest fullerene C_{20} ,³⁷ fullerenes are made solely of carbon and exhibit uncommon cage geometries. These extraordinary features of fullerenes are interesting on their own. What is surprising from an electronic structure standpoint is that many of these fullerenes exhibit complex generalized Hartree-Fock (cGHF) solutions as discovered by Jiménez-Hoyos et al.³⁸ These symmetry-broken cGHF solutions were interpreted as an indicator of polyradicaloid character of fullerenes. This is unexpected because experimentally synthesized fullerenes are quite stable and thus these stable ones are likely closed-shell in character.

The most striking conclusion of Jiménez-Hoyos and co-workers' work is that buckminsterfullerene, C_{60} , is polyradicaloid because of the existence of a cGHF solution. This contradicts with our group's previous attempt at characterizing the electron correlation of C_{60} . Our group discovered a restricted (R) to unrestricted (U) instability in C_{60} at the HF level.²⁹ We carefully assessed the nature of spin-symmetry breaking in comparison with C_{36} which is known to be strongly correlated. For C_{60} RMP2 yielded a more reasonable single-triplet gap than UMP2 and scaled opposite spin OOMP2 restored the spin-symmetry. For these reasons, our conclusion was that C_{60} is not strongly correlated and should be described as a closed-shell molecule.

In this work, we address this controversy on symmetry breaking of C_{60} and characterize the electron correlation of related molecules (i.e., C_{20} and C_{36}) using the recently developed regularized OOMP2 (κ -OOMP2)³⁵ and coupled-cluster valence bond with singles and doubles (CCVB-SD) methods.^{39,40}

2 Theory

We will use i, j, k, l, \dots to index occupied orbitals, a, b, c, d, \dots to index virtual orbitals, and p, q, r, s, \dots to index either of those two. n_α denotes the number of α electrons, n_β denotes the number of β electrons, n_{mo}^σ is the number of molecular orbitals of spin σ , and n_{so} is the number of spin orbitals.

2.1 Classification of HF Solutions

Fukutome pioneered the group-theoretic classification of non-relativistic HF solutions.⁴¹ There are a total of eight distinct classes based on the symmetry of the electronic Hamiltonian (complex conjugation (\hat{K}), time-reversal ($\hat{\Theta}$), and spin-operators $\hat{S}_{\mathbf{n}}$ where \mathbf{n} is a collinear axis and \hat{S}^2). We will follow the classification by Stuber and Paldus,⁴² which is identical to Fukutome’s classification with a different name for each class. The eight different classes are: restricted HF (RHF), complex RHF (cRHF), unrestricted HF (UHF), complex UHF (cUHF), generalized HF (GHF), and complex GHF (cGHF) along with paired UHF (pUHF) and paired GHF (pGHF). For the purpose of this work, we discuss symmetry breaking of \hat{K} , $\hat{S}_{\mathbf{n}}$, and \hat{S}^2 and do not discuss $\hat{\Theta}$. Therefore, there is no distinction between complex solutions and paired solutions since they differ only by time-reversal symmetry. We will thus discuss a total of six classes of HF solutions of each fullerene presented below.

2.2 Generalized MP2

GHF eliminates the distinction between α and β spin orbitals characteristic of UHF.^{41–46} Instead each electron occupies a spin-orbital that can be an arbitrary linear combination of α and β basis functions. We refer to such an orbital as a generalized spin-orbital (GSO). The usual spin-orbital MP2 energy expression reads,

$$E_{\text{MP2}} = E_0 - \frac{1}{4} \sum_{ijab} \frac{|\langle ij||ab \rangle|^2}{\Delta_{ij}^{ab}}, \quad (1)$$

where E_0 is the energy of the reference HF determinant the remainder is the MP2 correlation energy. Δ_{ij}^{ab} is a non-negative orbital energy gap defined as

$$\Delta_{ij}^{ab} = \epsilon_a + \epsilon_b - \epsilon_i - \epsilon_j, \quad (2)$$

and a two-electron integral $(ia|jb)$ is

$$(ia|jb) = \int_{\mathbf{r}_1, \mathbf{r}_2} \frac{\phi_i(\mathbf{r}_1)^* \phi_a(\mathbf{r}_1) \phi_j(\mathbf{r}_2)^* \phi_b(\mathbf{r}_2)}{|\mathbf{r}_1 - \mathbf{r}_2|_2}. \quad (3)$$

and an antisymmetrized integral is

$$\langle ij||ab \rangle = (ia|jb) - (ib|ja) \quad (4)$$

The evaluation of a two-electron integral with GSOs can be achieved in the following way:

$$(ia|jb) = (i^\alpha a^\alpha | j^\alpha b^\alpha) + (i^\alpha a^\alpha | j^\beta b^\beta) + (i^\beta a^\beta | j^\alpha b^\alpha) + (i^\beta a^\beta | j^\beta b^\beta) \quad (5)$$

where we used the fact that each GSO, $|\phi_p\rangle$, has an α and a β component

$$|\phi_p\rangle = \begin{pmatrix} \phi_p^\alpha \\ \phi_p^\beta \end{pmatrix}. \quad (6)$$

Having expanded out the two-electron integral this way, the implementation of GMP2 is (at least conceptually) trivial on top of an existing MP2 program.

The resolution of the identity approximation can be also applied to Eq. (5) using^{47,48}

$$(i^{\sigma_1} a^{\sigma_1} | j^{\sigma_2} b^{\sigma_2}) = \sum_{PQ} (i^{\sigma_1} a^{\sigma_1} | P)(P|Q)^{-1}(Q|j^{\sigma_2} b^{\sigma_2}) \quad (7)$$

where $(i^{\sigma_1} a^{\sigma_1} | P)$ represents a 2-electron 3-center Coulomb integral and $(P|Q)$ is the metric matrix of the above decomposition which is a 2-electron 2-center Coulomb integral among auxiliary basis functions.

The scaling of RI-cGMP2 is the same as RI-RMP2 or RI-UMP2 (i.e., $\mathcal{O}(N^5)$). However, it carries a large prefactor compared to RI-RMP2 or RI-UMP2. The bottleneck of RI-MP2 is forming two-electron integrals in Eq. (7). In the case of RI-RMP2 this step scales $\mathcal{O}(n_\alpha^2(n_{\text{mo}}^\alpha - n_\alpha)^2 n_{\text{aux}})$ whereas RI-UMP2 scales $\mathcal{O}((n_\alpha^2(n_{\text{mo}}^\alpha - n_\alpha)^2 + n_\beta^2(n_{\text{mo}}^\beta - n_\beta)^2 + n_\alpha n_\beta(n_{\text{mo}}^\alpha - n_\alpha)(n_{\text{mo}}^\beta - n_\beta)) n_{\text{aux}})$. Assuming $n_\alpha = n_\beta$, RI-UMP2 is three times more expensive than RI-RMP2. In the case of RI-GMP2, we have a scaling of $\mathcal{O}(n_{\text{elec}}^2(n_{\text{so}} - n_{\text{elec}})^2 n_{\text{aux}})$. Assuming $n_{\text{elec}} = 2n_\alpha$ and $n_{\text{so}} = 2n_{\text{mo}}^\alpha$, we conclude that RI-GMP2 is 16 times more expensive than RI-RMP2. RI-cGMP2 carries an extra factor of four due to complex arithmetic operations. Overall, RI-cGMP2 is 64 times more expensive than RI-RMP2. Since we will be studying reasonably large systems, this non-negligible prefactor will limit the applicability of RI-cGMP2 in this study.

We will use the RI approximation throughout this work so we shall drop ‘‘RI’’ and refer to ‘‘RI-MP2’’ as ‘‘MP2’’.

2.3 Regularized Orbital-Optimized MP2

When orbital-optimizing Eq. (1), it is commonly observed that the energy tends to $-\infty$. This divergence is attributed to the development of a small denominator, $\Delta_{ij}^{ab} \rightarrow 0$ for some i, j, a, b . While simple level shift were first explored^{33,34} they proved inadequate. To better

mitigate this problem, we proposed a regularized MP2 method whose energy reads

$$E_{\text{MP2}}(\kappa) = E_0 - \frac{1}{4} \sum_{ijab} \frac{|\langle ij||ab \rangle|^2}{\Delta_{ij}^{ab}} \left(1 - e^{-\kappa \Delta_{ij}^{ab}}\right)^2 \quad (8)$$

where $\kappa > 0$ is a single empirical parameter that controls the strength of regularization. The exponential damping function ensures that small denominators cannot contribute to the final energy. Orbital-optimizing Eq. (8) yields κ -OOMP2 which we thoroughly analyzed and benchmarked in our previous work.³⁵ $\kappa = 1.45 E_h^{-1}$ was recommended as it appeared to combine favorable recovery of Coulson-Fischer points with good numerical performance. We will also employ its scaled correlation energy variant, κ -S-OOMP2, where the optimal scaling parameter, c , for each $\kappa \in [0.05, 4.0]$ was determined in our previous work.³⁵

2.4 Classification of OOMP2 Solutions

The classification of OOMP2 solutions can be done in the same way as that of HF solutions. The classification needs to incorporate the MP2 correction to the one-particle density matrix (1PDM) and the first-order correction to the spin expectation values.

The norm of the imaginary part of the 1PDM, ξ , diagnoses the fundamental complexity of a wavefunction at the one-body level.⁴⁹ This was sufficient for testing the fundamental complexity of OOMP2 solutions studied in this work. In principle, one may consider a more sophisticated diagnostic tool that involves higher order density matrices.

The first-order correction to the spin expectation values are needed to compute the first-order correction to a spin covariance matrix \mathbf{A} defined as

$$A_{ij} = \langle \hat{S}_i \hat{S}_j \rangle - \langle \hat{S}_i \rangle \langle \hat{S}_j \rangle \quad (9)$$

The nullity of this matrix determines the collinearity of a given wavefunction as noted by Small et al.⁴⁵ If there is a zero eigenvalue associated with an eigenvector \mathbf{n} , the wavefunction

is collinear along this axis \mathbf{n} . The real part of \mathbf{A} is a positive semidefinite matrix and the smallest eigenvalue, μ_0 , can be used to quantify the non-collinearity of a given wavefunction. This applies to not only non-interacting wavefunctions such as HF states but also correlated states such as MP1 wavefunctions. We present the formula for computing the first-order correction to \mathbf{A} in the Appendix.

As a side note, during the course of finishing this work, we found that the expression for the first-order correction to $\langle \hat{S}^2 \rangle$ presented in ref. 14 is off by a factor of two and the one in ref. 32 is off by a factor of four from the correct expression. This is clear from looking at a more general expression given in the Appendix.

2.5 Coupled-Cluster Methods

Restricted CC with singles and doubles (RCCSD) generally fails to describe strongly correlated systems and often exhibits non-variationality in such systems. Recently, we proposed coupled-cluster valence bond with singles and doubles (CCVB-SD) as a simple alternative that modifies the parametrization of quadruple excitations in RCCSD.³⁹ CCVB-SD is better than RCCSD at handling strong correlation as it can describe bond dissociations exactly within a valence active space as long as UHF (or UCCSD) can. This property is inherited from a much simpler correlation model, CCVB.⁵⁰⁻⁵⁵ Furthermore, CCVB-SD was successfully applied to oligoacenes which exhibit emergent strong correlations while RCCSD showed non-variationality.⁴⁰ It is clear from our experience that strong correlation is present when we observe qualitative differences between CCVB-SD and RCCSD. This can be shown in terms of working equations. CCVB-SD modifies the quadruples in RCCSD which plays a crucial role in describing strong correlation. This modification becomes negligible if no substantial connected quadruples are needed and therefore in such cases there is no strong correlation. Comparing those CC methods will shed light on the electron correlation effects in the fullerenes.

3 Probes for Artificial Symmetry Breaking

3.1 Probe 1: Symmetry Breaking Landscape from κ -S-OOMP2

One way to address the problem of distinguishing between essential symmetry breaking (driven by missing static correlation effects) and artificial symmetry breaking (driven by missing dynamical correlation effects) in HF calculations is to apply a method that optimizes the orbitals including only dynamical correlation but not the static or essential correlation. With such an approach, artificial symmetry breaking will be virtually eliminated because dynamic correlation effects are explicitly included and are therefore removed as a driving force for symmetry breaking. Essential symmetry breaking remains because no static correlation is included to handle strong correlation problems.

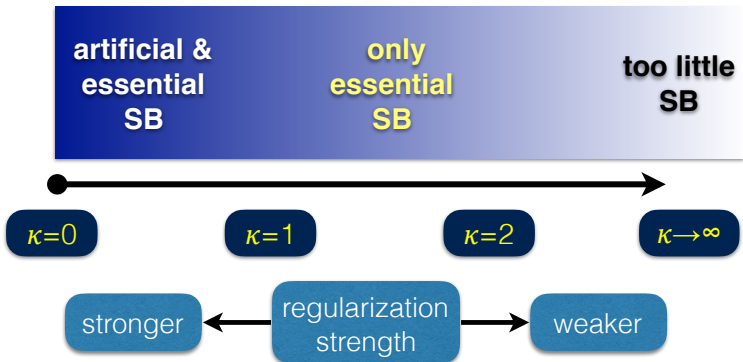


Figure 2: Illustration of artificial and essential symmetry breaking (SB) in κ -S-OOMP2 as a function of κ . $\kappa \in [1.0, 2.0]$ exhibits only essential SB.

The κ -S-OOMP2 method is such a theory for reasons that are summarized in Figure 2. Varying the regularization parameter over the range $[0.5, 4.0]$ for which this method has been parameterized yields a survey of how symmetry breaking depends on regularization strength. Regularization that is weak ($\kappa > 2$) defines methods that strongly favor symmetry-restoration, and will often be below the true energy. For example, in bond-breaking, Coulson-Fischer points are pushed to very long bond-lengths, and eventually are even lost. This arises because weak regularization includes part of the exaggerated MP2 description of the

(potentially strong) paired correlations associated with small promotion energies. Thus the limit of very weak regularization ($\kappa \rightarrow \infty$) may not even admit essential symmetry breaking for strongly correlated systems.

By contrast regularization that is strong ($\kappa < 1$) will potentially admit both essential and artificial symmetry breaking, because part of the dynamical correlation is also attenuated. This is most clearly seen by considering κ -OOMP2 without scaling, where the limit as $\kappa \rightarrow 0$ recovers HF theory, with all its symmetry breaking characteristics. Using the scaled method, κ -S-OOMP2, yields methods that have a somewhat lower driving force for symmetry breaking with small κ . Finally, the intermediate regime, which we view here as roughly $\kappa \in [1.0, 2.0]$, presents a transition between strong and weak regularization. The value of $\kappa = 1.45$ which was selected to yield useful accuracy and restore Coulson-Fischer points, as discussed previously,³⁵ lies in this region.

We can use the κ -dependence of symmetry breaking in κ -S-OOMP2 to characterize its nature. For an even electron system that exhibits symmetry breaking at the HF level, using κ -S-OOMP2 at a fixed geometry as a function of κ will yield a critical value, κ_c above which symmetry restoration is complete. If κ_c is large enough (weak regularization, for instance $\kappa_c > 2$), so that Coulson-Fischer points are not properly restored in bond-breaking, then we conclude that the HF symmetry breaking was essential in character, since so too is that of κ -S-OOMP2. On the other hand, if κ_c is small enough (strong regularization, for instance $\kappa_c < 1$) then we are well into the regime where Coulson-Fischer points exist, and we must therefore conclude that the HF symmetry breaking was artificial in character, because symmetry breaking is readily quenched in κ -S-OOMP2, even with strong regularization.

3.2 Probe 2: Singlet-Triplet Gap

A singlet-triplet gap measures the energy cost for breaking a pair of electrons that are singlet coupled. This would be much smaller than a usual single bond energy if two electrons are spatially well separated and singly occupying each orbital. This is the case for biradicaloids

where singlet-triplet gaps less than 10 kcal/mol are commonly observed.⁵⁶ On the other hand, if the gap is large then the molecule is best described as a closed-shell molecule. A precise experimental value for this gap is available for C₆₀ and therefore this is a good probe especially for C₆₀.

3.3 Probe 3: Correlated 1PDM

We will investigate two quantities that can be obtained from the correlated 1PDM of CC wavefunctions (RCCSD and CCVB-SD). The first one is natural orbital occupation numbers (NOONs) which are eigenvalues of the 1PDM. For a perfect closed-shell molecule, the NOONs would be either 0.0 (empty) or 2.0 (doubly occupied). For a perfect biradical system, there should be two eigenvalues of 1.0 as well. In general, the NOONs will be distributed between 0.0 and 2.0. A polyradicaloid must have multiple eigenvalues that significantly deviate from 0.0 and 2.0.

The second quantity that we will report is Head-Gordon’s number of unpaired electrons (NUE),⁵⁷

$$\text{NUE} = \sum_i \min(2 - n_i, n_i) \quad (10)$$

where i is summed over all natural orbitals and n_i is the occupation number of the i -th natural orbital. This takes the entire spectrum of NOONs and reduces it to a single scalar value that quantifies strong correlation. In the case of a perfect closed-shell molecule, NUE is zero. Molecules with open-shell character will exhibit larger NUE values. When these quantities show a qualitative difference between RCCSD and CCVB-SD for a given system, we conclude that the system is strongly correlated and vice versa.

4 Results

We investigated the C₆₀, C₃₆, and C₂₀ fullerenes. We studied a total of five different geometries of C₂₀ whereas only one conformation for other fullerenes was studied. All HF

calculations were performed with wavefunction stability analysis to ensure the local stability of solutions. The pertinent cGHF electronic Hessian is provided in the Appendix. All calculations were carried out with a development version of Q-Chem.⁵⁸ All correlation calculations employed the frozen core approximation for the sake of computational efficiency. All the plots were generated with Matplotlib⁵⁹ and all the molecular figures were generated with Chemcraft.⁶⁰

Obtaining quantitatively accurate answers with CC methods is very computationally intensive for fullerenes so we look for qualitative answers by comparing them to various OOMP2 methods. We will employ the STO-3G basis set in order to exaggerate the effect of strong correlation and discuss the implication within this basis set. We only present the CC data for C₆₀ and C₃₆ here; the CC data for C₂₀ showed the same conclusions as the other analyses based on OOMP2 we present below.

4.1 The Nature of Electron Correlation in C₆₀

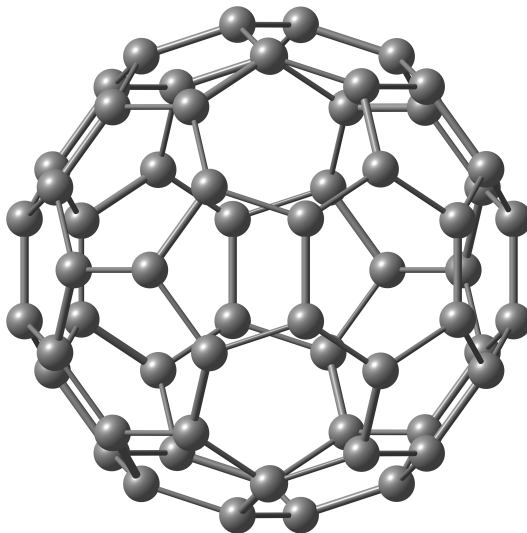


Figure 3: The I_h molecular structure of C₆₀.

C₆₀ is a well-known electron paramagnetic resonance silent molecule⁶¹ and its geometry is shown in Figure 3. Therefore, it is undoubtedly a molecule with a singlet ground state. Furthermore, its stability has suggested that it is a closed shell molecule.⁶² This is why

it was surprising to observe the existence of R to U symmetry breaking of C_{60} at the HF level.²⁹ This R to U symmetry breaking was in the end characterized as artificial based on analyses using OOMP2 and the single-triplet gap. Later, Jiménez-Hoyos et al. found a cGHF solution for C_{60} and concluded that C_{60} is strongly correlated (or polyradicaloid) based on this broken-symmetry HF solution.³⁸ This was surprising to us because C_{60} has been hardly suggested to be polyradicaloid and is also very stable in experiments. Therefore, we revisit this problem with κ -OOMP2 and CC methods and try to determine whether C_{60} is strongly correlated.

4.1.1 Symmetry Breaking Landscape

Due to limited computational time, we could obtain the symmetry breaking landscape of this molecule only within a minimal basis set, STO-3G.⁶³ We took the cGHF optimized geometry of C_{60} from Jiménez-Hoyos and co-workers’ work. As it is well known, the STO-3G basis set exaggerates strong correlation and facilitates symmetry breaking. The critical κ values obtained from minimal basis set calculations would therefore be a good estimate on the upper bound of κ_c .

In Figure 4, we present the symmetry breaking landscape of C_{60} . For $\kappa < 1.0$, $\langle S^2 \rangle_0$, ξ_0 , and μ_0 exhibit a steep increase as κ decreases. Eventually, the curve reaches the cGHF solution at the limit of $\kappa \rightarrow 0$. $\kappa = 1.0$ is enough to restore all symmetries that were broken at the HF level. This critical value is not in the range of essential symmetry breaking illustrated in Section 3.1. Therefore we conclude that the symmetry breaking at the HF level is *artificial*. We also confirmed the symmetry restoration at $\kappa = 1.45$ with κ -OOMP2 within the VDZ (i.e., cc-pVDZ⁶⁴ without polarization) basis set. Therefore, we believe that the basis set incompleteness error will not affect this qualitative conclusion.

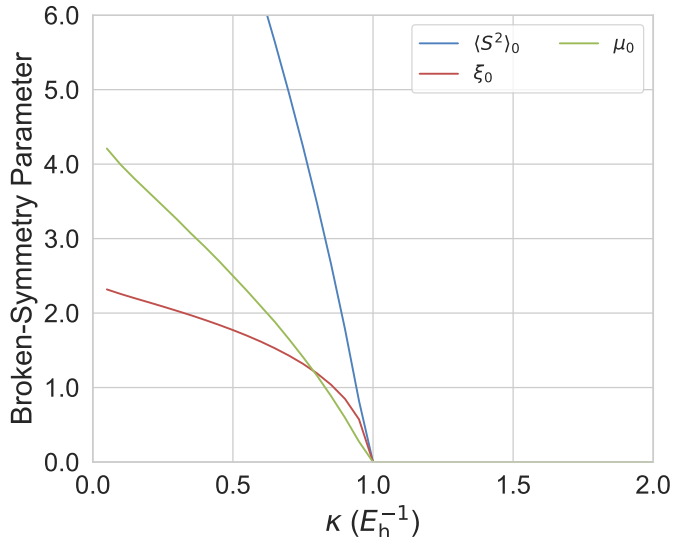


Figure 4: Measures of symmetry breaking ($\langle S^2 \rangle_0$, ξ_0 , and μ_0) as a function of the regularization strength κ for C_{60} (I_h). It should be noted that these plots are obtained with a scaled correlation energy variant of κ -OOMP2 (i.e., κ -S-OOMP2). These quantities do not include correlation corrections: in other words, the plots characterize symmetry-breaking/restoration in the reference determinant.

Table 1: The singlet-triplet gap ΔE_{S-T} (kcal/mol) of C_{60} from various methods. The expectation values of $\langle \hat{S}^2 \rangle$ for $M_S = 0$ and $M_S = 1$ states are presented as well. Note that these values include correlation corrections to $\langle \hat{S}^2 \rangle$.

Method	ΔE_{S-T}	$\langle \hat{S}^2 \rangle_{M_S=0}$	$\langle \hat{S}^2 \rangle_{M_S=1}$
RHF	65.63	0.000	2.000
RMP2	50.19	0.000	2.000
SCS-RMP2	52.21	0.000	2.000
SOS-RMP2	53.22	0.000	2.000
UHF	45.23	6.708	8.560
UMP2	77.39	5.566	7.401
UOOMP2	19.48	0.000	2.043
SCS-UOOMP2	28.53	0.000	2.002
SOS-UOOMP2	35.72	0.000	1.995
κ -UOOMP2	49.23	0.000	2.002
Experiment ⁶⁵	36.95 ± 0.02		

4.1.2 Singlet-Triplet Gap

In Table 1, we present the singlet-triplet gap of C_{60} computed with various MP2 methods. Here, we used the cc-pVDZ basis set⁶⁴ along with the corresponding auxiliary basis set.⁶⁶ For

OO methods, we performed orbital optimization starting from stable UHF solutions. The results presented in Table 1 generally agree with what Stück and Head-Gordon reported.²⁹

The singlet-triplet gap predicted by HF is better with UHF (45.23 kcal/mol) than with RHF (65.63 kcal/mol) in comparison to the experimental value (36.95 ± 0.02 kcal/mol). UHF exhibits striking spin-contamination and this is improved to a small extent with UMP2. The singlet-triplet gap of UMP2 is much worse than that of UHF, going from 45.23 kcal/mol to 77.39 kcal/mol whereas RMP2 improves the gap by 15 kcal/mol compared to RHF. It is clear that a better reference for subsequent correlation calculations is RHF not UHF. We also compare RMP2 with spin-component scaled MP2⁸⁰(SCS-MP2) and scaled opposite-spin MP2⁸¹ (SOS-MP2). The singlet-triplet gap is quite insensitive to the choice of scaling factors.

OOMP2 methods successfully remove heavy spin-contamination observed at the HF level. While in terms of $\langle \hat{S}^2 \rangle$ unregularized OOMP2 and its scaled variants are desirable, a striking underestimation of the gap is alarming. In particular, compared to their non-OO variants these gaps are severely underestimated. We suspect that this is due to overcorrelating the $M_S = 1$ state via OO. Unlike the non-OO variants, unregularized (i.e., $\kappa \rightarrow \infty$) OO methods are sensitive to the scaling parameters. We observe that the gap from SOS-UOOMP2 is only off by 1 kcal/mol from the experimental value. This is likely a fortuitous outcome.

It is interesting that this unphysical overcorrelation of the triplet state seems to be successfully resolved with κ -UOOMP2. κ -UOOMP2 yields more or less the same singlet-triplet gap as that of RMP2. κ -UOOMP2 exhibits an error of 12 kcal/mol which is likely due to the limited treatment of electron correlation. It will be interesting to resolve this remaining error using higher order perturbation theory or, perhaps, coupled-cluster methods.

4.1.3 Correlated 1PDM

We then obtain NOONs from OOMP2 methods and analyze them. We will discuss three unregularized OOMP2 methods, OOMP2, SCS-OOMP2,³¹ and SOS-OOMP2¹⁴ along with

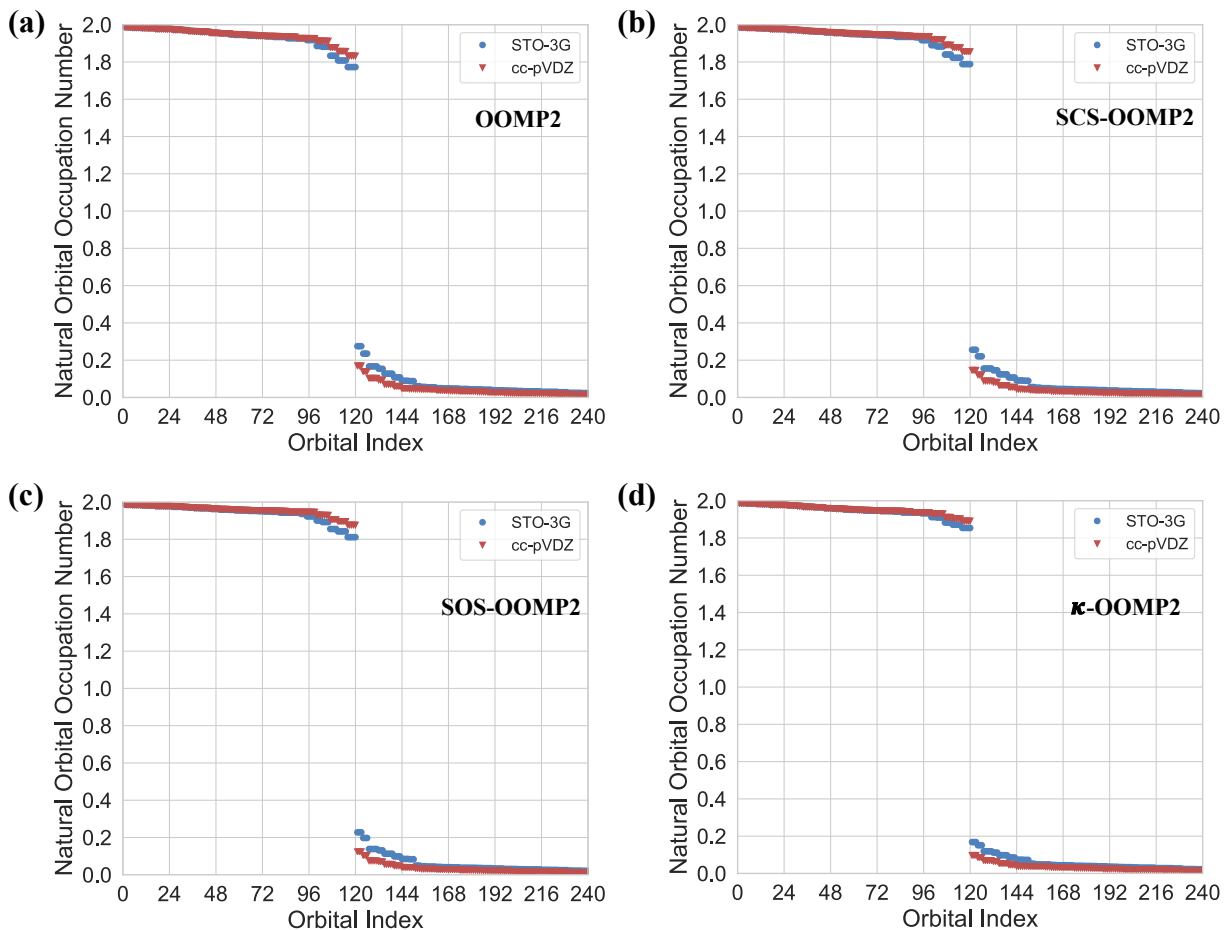


Figure 5: Natural orbital occupation numbers of C_{60} within a valence active space from (a) OOMP2, (b) SCS-OOMP2, (c) SOS-OOMP2, and (d) κ -OOMP2. Note that there were no unrestricted solutions found for any of these methods.

κ -OOMP2. In Figure 5, different OOMP2 methods exhibit more or less identical NOONs. We could not find unrestricted solutions for any of these methods. This reflects the simplicity of the electronic structure of C_{60} . A slight reduction in open-shell character is observed in κ -OOMP2 compared to other OOMP2 methods. These NOONs are far from the usual values for orbitals with open-shell character in strongly correlated wavefunctions (i.e., values between 1.30 and 0.70).

Likewise, the NOONs from CC methods presented in Figure 6 strongly suggest that this molecule is *not strongly correlated*. RCCSD and CCVB-SD exhibit visually identical distributions. Indeed, the NOONs of the highest occupied NO (HONO) and the lowest

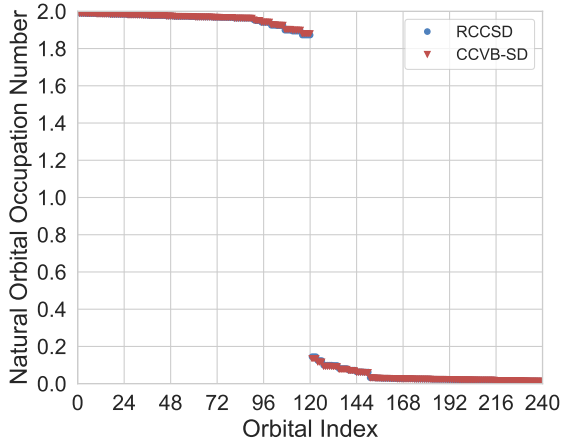


Figure 6: Natural orbital occupation numbers of C_{60} within the minimal basis set, STO-3G, from RCCSD and CCVB-SD. Two sets of data points are very close to each other so the blue circles lie right below the red triangles.

unoccupied NO (LUNO) are (1.87, 0.14) for both methods. These values are comparable to naphthalene’s NOONs computed with CCVB-SD. Evidently, naphthalene is not a strongly correlated system, which implies that neither is C_{60} .

Table 2: Number of unpaired electrons (NUE) of C_{60} computed from various methods. The numbers in parentheses are NUE per carbon atom.

Method	STO-3G	cc-pVDZ
OOMP2	16.07 (0.27)	13.99 (0.23)
SCS-OOMP2	15.32 (0.26)	12.59 (0.21)
SOS-OOMP2	13.82 (0.23)	10.99 (0.18)
κ -OOMP2	12.93 (0.22)	11.61 (0.19)
RCCSD	9.48 (0.16)	
CCVB-SD	9.19 (0.15)	

In Table 2, we present NUEs (Eq. (10)) of C_{60} computed by various methods. With a larger basis set (cc-pVDZ), NUEs are smaller than those of STO-3G. This reflects the reduction in strong correlation with the increase in the basis set size. We once again observe almost no differences between RCCSD and CCVB-SD. Overall, there are about 0.20 unpaired electrons per C atom in C_{60} . As each C atom has four valence electrons, this amounts only 5% of the total number of electrons. Therefore, the polyradicaloid character in C_{60} is only marginal from the global electronic structure viewpoint.

Based on these analyses, we conclude that C_{60} should be considered a closed-shell molecule and *not strongly correlated*. Thus the very interesting cGHF solution reported previously³⁸ should be considered as an artificial rather than an essential symmetry breaking. This conclusion will be also supported by comparing with our next molecule, C_{36} which is a well-known biradicaloid.

4.2 The Nature of Electron Correlation in C_{36}

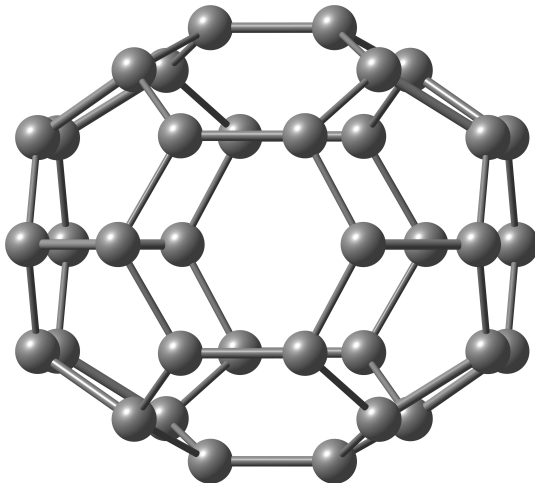


Figure 7: The D_{6h} molecular structure of C_{36} .

The D_{6h} structure of C_{36} shown in Figure 7 has been known to exhibit strong biradicaloid character.⁶⁷ This has been of great interest both experimentally⁶⁸ and theoretically.^{67,69–75} The D_{6h} structure is supported by the ^{13}C NMR spectrum exhibiting a single peak.⁶⁸ Different computational methods suggested different structures and even different multiplicities. There is no doubt that C_{36} exhibits complex electronic structure and is a strongly correlated system.

Stück and Head-Gordon studied this prototypical strongly correlated system using unregularized SOS-OOMP2 before. Fortunately, unregularized OOMP2 did not diverge even with this substantial biradicaloid character. What was not explicitly mentioned in this previous work is that OOMP2 in fact yields a restricted solution when starting from an unrestricted

solution. Since unregularized OOMP2 unphysically prefers restricted solutions (closely connected to its singularity problem), this is not unexpected. This also suggests that whether unregularized OOMP2 restores broken symmetry is not a definitive probe to characterize strong electron correlation in a given system (it is the $\kappa \rightarrow \infty$ limit shown in Fig. 2). We will see how κ -OOMP2 resolves this artifact and can be used to probe strong correlation in this system.

We obtained the D_{6h} molecular structure of C_{36} via geometry optimization with restricted density functional calculations using the BLYP exchange-correlation functional^{76,77} and the 6-31G(d) basis set.⁷⁸ The geometry optimization was performed with a D_{6h} geometric constraint so the optimization was not allowed to break this spatial symmetry. We do not think that this geometry is quantitatively accurate but for the purpose of this work, it should be sufficient.

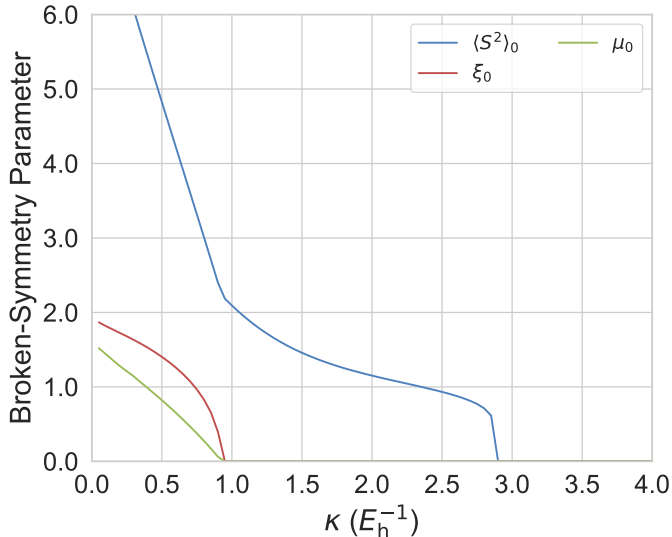


Figure 8: Measures of symmetry breaking ($\langle S^2 \rangle_0$, ξ_0 , and μ_0) as a function of the regularization strength κ for C_{36} (D_{6h}). It should be noted that these plots are obtained with a scaled correlation energy variant of κ -OOMP2 (i.e., κ -S-OOMP2). These quantities do not include correlation corrections: in other words, the plots characterize symmetry-breaking/restoration in the reference determinant.

4.2.1 Symmetry Breaking Landscape

We computed a landscape of symmetry breaking as a function of κ within the 6-31G basis set⁷⁹ along with the cc-pVDZ auxiliary basis set.⁶⁶ This may not be quantitatively accurate, but it should be enough to draw qualitative conclusions. Figure 8 shows that C_{36} exhibits multiple classes of one-particle wavefunctions as a function of κ . As noted by Jiménez-Hoyos et al.,³⁸ at the HF level there exists a cGHF solution. This is clearly evident in Figure 8 for $\kappa < 0.95$, since we have nonzero $\langle S^2 \rangle_0$, ξ_0 , and μ_0 . ξ_0 and μ_0 vanish at their critical value $\kappa_c = 0.95$ and only unrestricted solutions were obtained for $\kappa \in [0.95, 2.85]$. For $\kappa > 2.85$, only restricted solutions were found. This is consistent with Stück and Head-Gordon’s work which used SOS-OOMP2.²⁹ This landscape has more structure than that of C_{60} (see Fig. 4) which reflects the increased complexity of the electronic structure of C_{36} .

The κ value within the essential symmetry breaking region exhibits only unrestricted solutions. Therefore, complex generalized and restricted solutions reflect artificial symmetry breaking. Since C_{36} is a well-known singlet biradicaloid, one would expect an unrestricted solution with an $\langle S^2 \rangle_0$ value between 0.0 and 2.0 (i.e., there is only triplet contaminant). Interestingly, this is what was obtained from κ -S-OOMP2 with $\kappa \approx 1.5$ and also from κ -OOMP2 with $\kappa = 1.45$ (see below). Based on the existence of this essential symmetry breaking, we conclude that C_{36} is strongly correlated.

4.2.2 Singlet-Triplet Gap

We will focus on determining whether unscaled κ -OOMP2 with $\kappa = 1.45$ (i.e., the recommended default κ -OOMP2 method³⁵) works quantitatively well compared to other MP2 approaches. We observed the same cG to U partial symmetry restoration with $\kappa = 1.45$ within the cc-pVDZ basis set. Therefore, due to limited computational resources, for the cc-pVTZ basis set^{64,66} we only ran unrestricted calculations. In Table 3, we present the singlet-triplet gap (ΔE_{S-T}) computed with various MP2 approaches. Since there is no reliable experimental gap available, we shall compare our results against multi-reference MP2

Table 3: The singlet-triplet gap ΔE_{S-T} (kcal/mol) of C_{36} from various methods. The expectation values of $\langle \hat{S}^2 \rangle$ for $M_S = 0$ and $M_S = 1$ states are presented as well. Note that these values include correlation corrections to $\langle \hat{S}^2 \rangle$. All but MRMP2 results were obtained with the cc-pVTZ basis set.⁶⁴ MRMP2 results in ref. 67 were obtained with a D_{6h} geometry within the 6-31G(d) basis set. MRMP2 was performed on a CASSCF solution with a (2e, 4o) active space.

Method	ΔE_{S-T}	$\langle \hat{S}^2 \rangle_{M_S=0}$	$\langle \hat{S}^2 \rangle_{M_S=1}$
RHF	-19.69	0.000	2.000
RMP2	14.46	0.000	2.000
SCS-RMP2	9.75	0.000	2.000
SOS-RMP2	7.40	0.000	2.000
UHF	32.29	7.448	8.793
UMP2	42.73	6.428	7.795
UOOMP2	15.85	0.000	2.070
SCS-UOOMP2	30.76	0.000	1.978
SOS-UOOMP2	22.91	0.000	2.002
κ -UOOMP2	4.42	0.959	2.008
AP+ κ -UOOMP2	8.46		
MRMP2 ⁶⁷	8.17		

(MRMP2) results.⁶⁷ The MRMP2 results were obtained with the 6-31G(d) basis set and a small active space, (2e, 4o), complete active space self-consistent field (CASSCF) reference state. These might not be a highly accurate reference result, but it can serve as a qualitative answer.

RHF predicts a triplet ground state, a qualitatively wrong result. RMP2, SCS-RMP2,⁸⁰ and SOS-RMP2⁸¹ correct the sign of the gap. They are also not too far away from the multi-reference MP2 (MRMP2) result and this is a fortuitous result given the singlet biradicaloid character of the true ground state cannot be captured by doubly occupying restricted orbitals. UHF and UMP2 are heavily spin-contaminated and predict significantly large gaps. We note that the MP2 treatment cannot clean up heavy spin-contamination present at the UHF level. As a result, these gaps are qualitatively incorrect as they are too large to support the singlet biradicaloid character.

Spin-contamination is successfully removed with unregularized OOMP2 methods. The UOOMP2 gap is quantitatively close to RMP2. However, SCS- and SOS-MP2 methods pre-

dict much larger gaps with OO than those without OO. This is likely due to overcorrelating the singlet state. This is the case where OOMP2 (or κ -OOMP2 for $\kappa \rightarrow \infty$) yields too little symmetry breaking as explained in Section 3.1.

κ -UOOMP2 yields a broken-symmetry solution for $M_S = 0$ and $\langle \hat{S}^2 \rangle$ is 0.959. This is of a strong singlet biradicaloid character and serves as a good candidate for Yamaguchi’s approximate spin-projection (AP)⁸² to obtain better energetics. The use of AP in conjunction with κ -UOOMP2 was first discussed in ref. 35. Without AP, the gap was predicted to be 4.42 kcal/mol. This is small enough to conclude that C_{36} is a singlet biradicaloid, but the gap is underestimated due to spin-contamination. Applying AP lowers the singlet energy by 4 kcal/mol which yields a gap of 8.46 kcal/mol. This is quite close to the reference MRMP2 energy. However, a more precise benchmark is highly desirable in the future to draw a more definitive conclusion. Nevertheless, the result suggests that C_{36} is strongly correlated which agrees with the conclusion drawn based on the symmetry breaking landscape.

4.2.3 Correlated 1PDM

In Figure 9, we discuss NOONs of C_{36} from the various OOMP2 methods that were used in the previous sections. For STO-3G, OOMP2, SOS-OOMP2, and κ -OOMP2 exhibit clear emergent singlet biradicaloid character. It is clear that NOONs exhibit more open-shell character than those of C_{60} . Interestingly, we could isolate an unrestricted STO-3G solution with SOS-OOMP2 by reading in an unrestricted κ -OOMP2 solution. We could not isolate such a solution with the cc-pVTZ basis set. The R to U symmetry breaking of SOS-OOMP2 is interesting in that the unrestricted solution seems to have more closed-shell orbitals than the restricted solution. Moreover, the unrestricted solution is 21 mE_h higher in energy than the restricted one. Within the cc-pVTZ basis set, OOMP2, SCS-OOMP2, and SOS-OOMP2 all predict very similar NOONs and they exhibit only slight singlet biradicaloid character. On the other hand, κ -OOMP2 exhibits very strong biradicaloid character characterized by an unrestricted solution. HONO and LUNO for this unrestricted solution have NOONs of

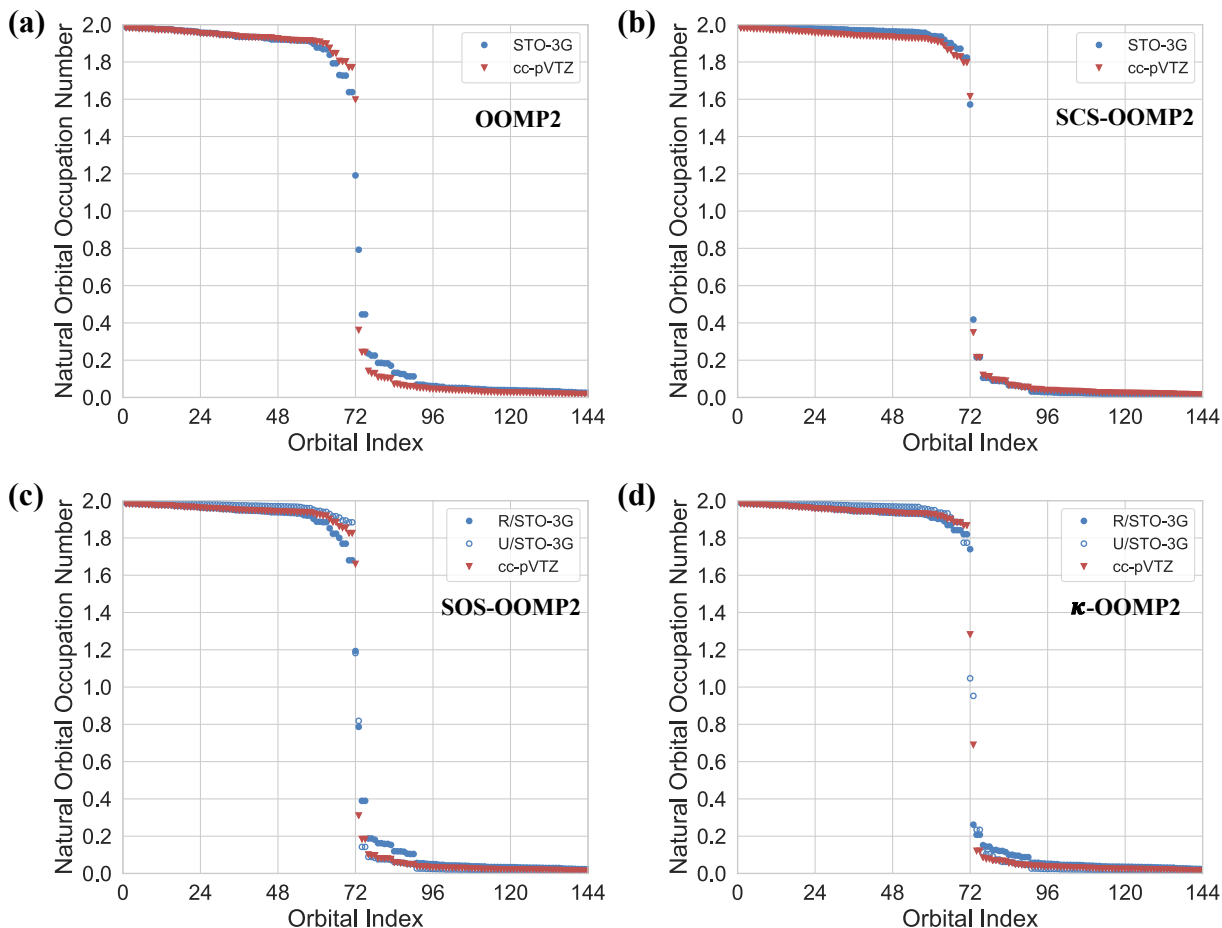


Figure 9: Natural orbital occupation numbers of C_{36} within the valence space from (a) OOMP2, (b) SCS-OOMP2, (c) SOS-OOMP2, and (d) κ -OOMP2. Note that there were no unrestricted solutions found for OOMP2 and SCS-OOMP2. Furthermore, the solution from κ -OOMP2 with cc-pVTZ is unrestricted.

1.28 and 0.69, respectively. The true ground state would have less polarized NOONs than κ -OOMP2.

In Figure 10, we show NOONs from two CC methods, RCCSD and CCVB-SD. As was noted before, RCCSD and CCVB-SD show qualitative differences when the system is strongly correlated.^{39,40} In particular, RCCSD clearly overcorrelates and likely exhibits non-variationality.⁴⁰ These trends are well reflected in Figure 10. The NOONs of the HONO and the LUNO are (1.35, 0.65) and (1.68, 0.32) for RCCSD and CCVB-SD, respectively. These two sets of NOONs show clear differences in that RCCSD exhibits far more open-shell character than does CCVB-SD. In passing we note that the CCVB-SD value (1.68, 0.32) is

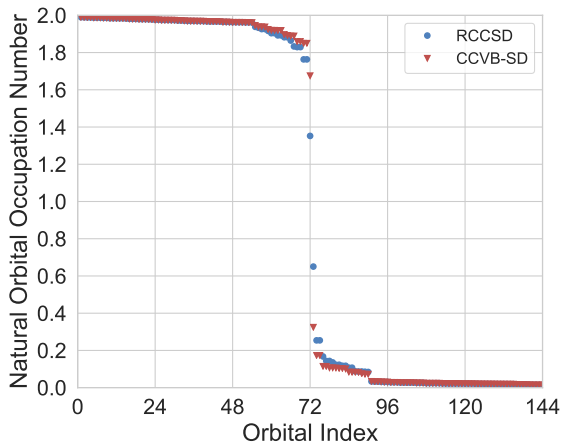


Figure 10: Natural orbital occupation numbers of C_{36} within the minimal basis set, STO-3G, from RCCSD and CCVB-SD.

comparable to NOONs of an acene of length 12 we studied in ref. 40. This is quite substantial strong correlation.

Table 4: Number of unpaired electrons (NUE) of C_{36} computed from various methods. For SOS-OOMP2 and κ -OOMP2 with STO-3G, we present NUE for both restricted and unrestricted solutions. The first value corresponds to the restricted one and the second corresponds to the unrestricted one. The numbers in parentheses are NUE per carbon atom. STO-3G/R indicates restricted calculations with STO-3G while STO-3G/U indicates unrestricted calculations with STO-3G. The cc-pVTZ calculations are done with spin-unrestricted calculations and broken symmetry solutions are indicated by a superscript 1. ¹ Spin-unrestricted solutions.

Method	STO-3G/R	STO-3G/U	cc-pVTZ
OOMP2	12.88 (0.36)	N/A	10.66 (0.30)
SCS-OOMP2	6.24 (0.17)	N/A	9.66 (0.27)
SOS-OOMP2	11.31 (0.31)	6.17 (0.17) ¹	8.44 (0.23)
κ -OOMP2	8.93 (0.25)	6.95 (0.19) ¹	9.25 (0.26) ¹
RCCSD	8.23 (0.23)	N/A	
CCVB-SD	6.65 (0.18)	N/A	

We present the NUEs computed from the various methods examined here in Table 4. SOS-OOMP2 and κ -OOMP2 exhibit smaller NUE with unrestricted solutions than with restricted solutions. This suggests that the spin polarization occurs within a few orbitals which in turn reduces the global correlation. This is in agreement with Figure 9. Compared to Table 2, all the NUEs are smaller with C_{36} than with C_{60} . However, this is simply due to

the fact that there are more electrons in C_{60} . With a proper normalization (i.e., NUE per C atom), it is clear that C_{60} exhibits less open-shell character than C_{36} .

For OOMP2 and SOS-OOMP2 (restricted), increasing the basis set size decreases the NUE values. The minimal basis set we used indeed provided more prominent open-shell character than cc-pVTZ in these methods. For κ -OOMP2 (unrestricted) and SCS-OOMP2, the open-shell character increases going from STO-3G to cc-pVTZ. Although HONO and LUNO exhibit less polarization, the other orbitals exhibit more open-shell character with a larger basis set. This can be understood as having more dynamic correlation effects and smaller correlation within a valence space in the cc-pVTZ basis set.

Comparing NUEs of RCCSD and CCVB-SD clearly suggests that RCCSD overcorrelates the system. Therefore, this also suggests that C_{36} is strongly correlated.

4.3 The Nature of Electron Correlation in C_{20}

Lastly, we obtain the landscape of symmetry breaking of a smaller fullerene, C_{20} . We have established that all three probes we used yield a consistent conclusion for C_{60} and C_{36} . Therefore, we believe that it is sufficient to use this single probe to obtain an answer to a qualitative question: is C_{20} strongly correlated?

4.3.1 Jahn-Teller distorted structures

C_{20} has attracted a lot of attention since it is the smallest possible fullerene suggested by graph-theoretic analyses.⁸³ The existence of its cage geometry was controversial for some time,⁸⁴⁻⁹¹ but eventually it was experimentally observed in 2000.³⁷ Since then, there have been a lot of quantum chemistry studies of C_{20} which focus on relative energetics of different conformers such as bowl, cage, and ring.^{75,92-97} Here we focus on multiple Jahn-Teller distorted conformations of the cage geometry (C_{2h} , D_{2h} , C_i , and D_{3h}).

Manna and Martin carried out a careful study of relative energies among the Jahn-Teller distorted conformers of C_{20} .⁹⁷ They used state-of-the-art wavefunction methods in

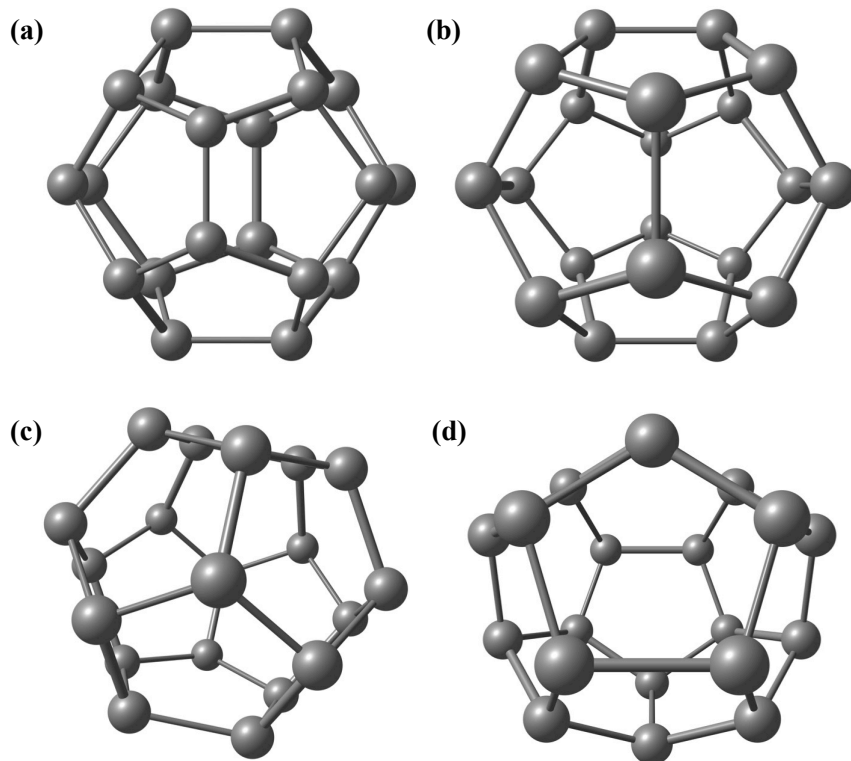


Figure 11: Four Jahn-Teller distorted isomers of C_{20} : (a) C_{2h} , (b) D_{2h} , (c) C_i , and (d) D_{3h} .

conjunction with high-quality density functional theory calculations. We took molecular geometries of C_{20} from ref. 97 which were optimized with PBE0 and the cc-pVTZ basis set. These geometries are shown in Figure 11. Our focus in this section is on the artificial symmetry breaking in these molecules. We studied these within the cc-pVDZ basis set⁶⁴ along with the appropriate auxiliary basis set.⁶⁶ In Table 5, we present the classification of HF solutions of these molecules. Since they are commonly thought of as closed-shell molecules, it is striking that RHF is always unstable under spin-symmetry breaking for these molecules.

Table 5: Classification of HF solutions of C_{20} isomers along with the corresponding $\langle S^2 \rangle_0$, ξ_0 , and μ_0 . The subscript 0 denotes that these properties are computed at the HF level.

Geometry	\hat{K}	\hat{S}^2	\hat{S}_n	Stuber-Paldus	$\langle S^2 \rangle_0$	ξ_0	μ_0
C_{2h}	Broken	Broken	Broken	cGHF	5.395	1.117	0.816
D_{2h}	Broken	Broken	Broken	cGHF	5.397	1.626	0.818
C_i	Broken	Broken	Conserved	cUHF	5.101	1.074	0.000
D_{3h}	Broken	Broken	Conserved	cUHF	5.100	1.247	0.000

We will first discuss the cGHF solutions found in C_{2h} and D_{2h} . Although the two geometries differ by 29 mE_h in terms of the nuclear repulsion energy, the cGHF energies differ only by 10 μ E_h. While this accidental electronic near-degeneracy is surprising, the appearance of non-collinear solutions is also striking since this molecule should be considered closed-shell.^{75,84,89,98} We will now see how regularized OOMP2 restores this artificial symmetry breaking starting from these broken symmetry solutions as a function of the regularization strength.

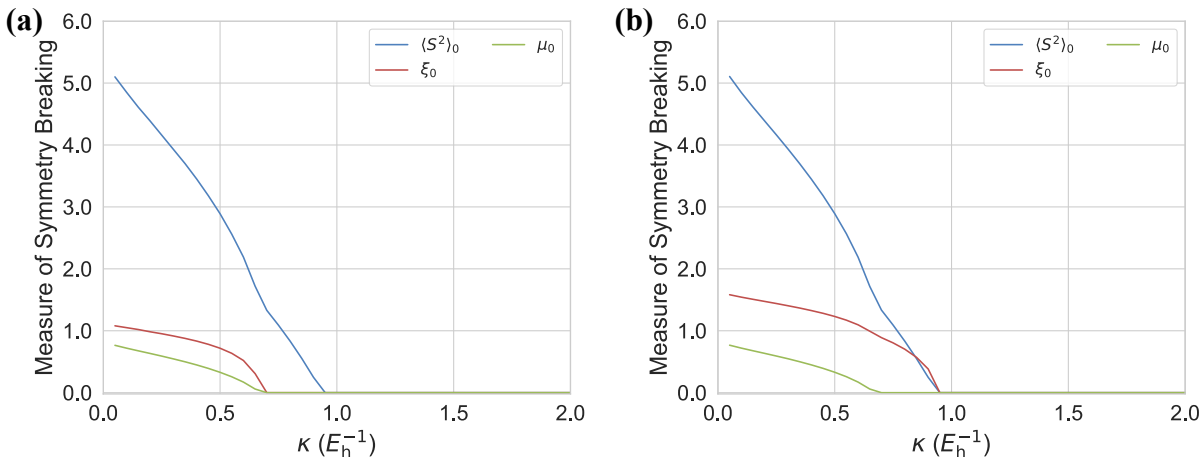


Figure 12: Measures of symmetry breaking ($\langle S^2 \rangle_0$, ξ_0 , and μ_0) as a function of the regularization strength κ for (a) C_{20} (C_{2h}) and (b) C_{20} (D_{2h}). It should be noted that these plots are obtained with a scaled correlation energy variant of κ -OOMP2 (i.e., κ -S-OOMP2). These quantities do not include correlation corrections: in other words, the plots characterize symmetry-breaking/restoration in the reference determinant.

In Figure 12, $\langle S^2 \rangle_0$, ξ_0 , and μ_0 are plotted as a function of κ for C_{2h} and D_{2h} geometries. Although two cGHF solutions exhibit quantitative similarity in $\langle S^2 \rangle_0$, ξ_0 , and μ_0 as shown in Table 5, κ_c values for each quantity shows a qualitative difference.

In the case of the C_{2h} geometry (Figure 12 (a)), κ_c values are 0.95, 0.70 and 0.70 for $\langle S^2 \rangle_0$, ξ_0 , and μ_0 , respectively. This suggests that for $\kappa \in [0.70, 0.95]$ there are unrestricted solutions for this system. Moreover, the symmetry restoration of complex and non-collinearity occurs at the same time. The $\langle S^2 \rangle_0$ restoration requires stronger MP2 correlation energies than ξ_0 and μ_0 . The D_{2h} geometry exhibits a different behavior. The κ_c values for $\langle S^2 \rangle_0$, ξ_0 , and

μ_0 are 0.95, 0.95, and 0.70, respectively. In this case, for $\kappa \in [0.70, 0.95]$ there are complex, unrestricted solutions. The U to G symmetry breaking is easier to restore than complex and unrestricted based on the relative magnitude of κ_c values. These κ_c values are in the artificial symmetry breaking range discussed in Section 3.1. Therefore, we conclude that this symmetry breaking is *artificial*.

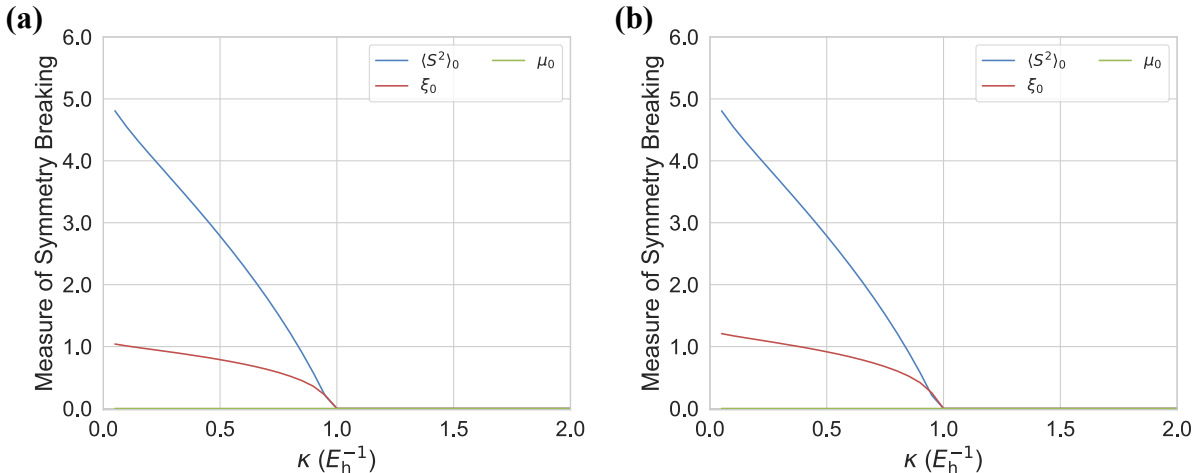


Figure 13: Measures of symmetry breaking ($\langle S^2 \rangle_0$, ξ_0 , and μ_0) as a function of the regularization strength κ for (a) C_{20} (C_i) and (b) C_{20} (D_{3h}). It should be noted that these plots are obtained with a scaled correlation energy variant of κ -OOMP2 (i.e., κ -S-OOMP2). These quantities do not include correlation corrections: in other words, the plots characterize symmetry-breaking/restoration in the reference determinant.

There are a total of two cUHF solutions in the C_i and D_{3h} geometries. The nuclear repulsion energies of these molecules differ by $29 \text{ m}E_h$ and the cUHF solutions differ only by $10 \text{ } \mu E_h$. This appearance of electronic degeneracy is similar to the two cGHF solutions of the same molecule. In Figure 13, the three measures of symmetry breaking is shown as a function of κ for these two geometries. Clearly, μ_0 is zero at every regularization strength so there is no generalized solution for these geometries. Although there were qualitative differences in κ_c between C_{2h} and D_{2h} , C_i and D_{3h} show identical κ_c values for $\langle \hat{S} \rangle_0$ and ξ_0 . The κ_c values are 0.95 for both of the symmetries, which is in the artificial symmetry breaking range. Therefore, this symmetry breaking should also be considered *artificial*.

We emphasize these findings about four different geometries of C_{20} agree with previ-

ous studies by others^{75,84,89,98}: C_{20} is a singlet closed-shell molecule and there is no strong correlation in this molecule as long as the geometry is Jahn-Teller distorted.

4.3.2 Dodecahedral (I_h) Structure

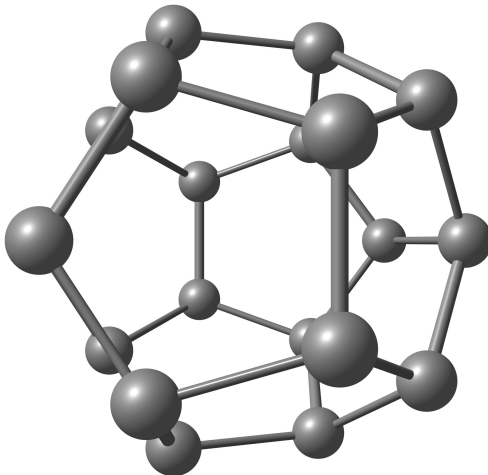


Figure 14: The dodecahedral molecular structure of C_{20} .

It is possible to force strong correlation by enforcing a higher symmetry. It is very likely that small fluctuations would be sufficient to break any degeneracies present in a higher symmetry and results into a more stable and lower symmetry geometry. This is the origin of commonly observed Jahn-Teller distortions. It is very surprising that a dodecahedral geometry (I_h) was found to be the global minimum with cGHF in the work by Jiménez-Hoyos et al.³⁸ We took the geometry from their work (shown in Figure 14) and ran the same analysis to see how symmetry breaking plays a role in describing the electron correlation of this molecule.

In Figure 15, we present a symmetry breaking landscape of the dodecahedral geometry. It has more structure than other previous cases. There is a discontinuous jump in μ_0 going from $\kappa = 1.00$ to $\kappa = 1.05$. This is due to the existence of two distinct low-lying solutions: complex, generalized and complex, unrestricted solutions. The gap between these two competing solutions is controlled by κ and around $\kappa = 1.00$ the relative energetics becomes reversed. For $\kappa > 1.00$, cU solutions are found to be the lowest energy solution.

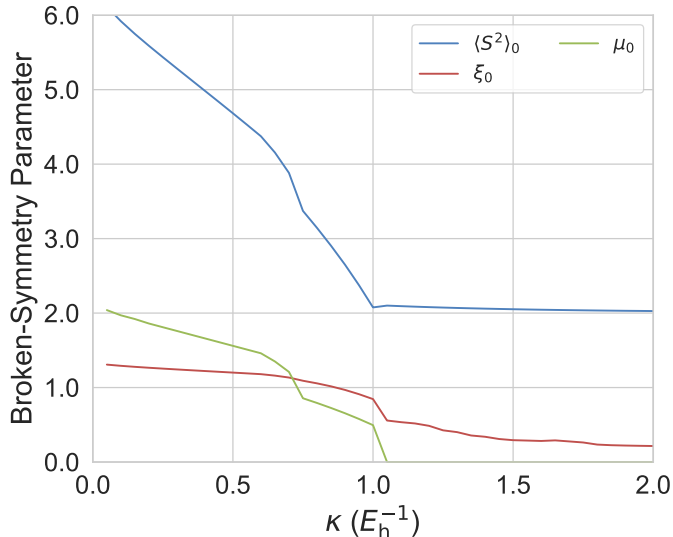


Figure 15: Measures of symmetry breaking ($\langle S^2 \rangle_0$, ξ_0 , and μ_0) as a function of the regularization strength κ for C_{20} with a dodecahedral geometry. It should be noted that these plots are obtained with a scaled correlation energy variant of κ -OOMP2 (i.e., κ -S-OOMP2). These quantities do not include correlation corrections: in other words, the plots characterize symmetry-breaking/restoration in the reference determinant.

$\langle \hat{S} \rangle_0$ suggests that a triplet state (with complexity) is the ground state of this system for reasonable κ values. At $\kappa = 1.45$, we examined the energy lowering from complexity by comparing the energy between U and cU solutions. We found that these solutions are degenerate as well.

This intricate landscape of symmetry breaking indicates that the system is likely strongly correlated under this geometry. Furthermore, a definitive answer to this question was obtained from equation-of-motion spin-flip coupled-cluster with singles and doubles (EOM-SF-CCSD) within the cc-pVDZ basis set starting from an $M_S = 1$ κ -OOMP2 orbitals. The $M_S = 1$ unrestricted CCSD calculation has $\langle \hat{S}^2 \rangle = 2.02$ which should serve as a good reference state for a subsequent spin-flip calculation. The EOM-SF-CCSD⁹⁹ calculation yielded a near-exact degeneracy between singlet and triplet states (i.e., near-zero singlet-triplet gap) and this strongly suggests that the system is strongly correlated. This is also consistent with the prediction by molecular orbital theory.¹⁰⁰

Therefore, we confirm that the claim by Jiménez-Hoyos et al. is correct that C_{20} at

the I_h geometry is strongly correlated. The next question is then whether this geometry is the actual ground state conformation of C_{20} . Given the near-zero singlet-triplet gap of the I_h geometry, C_{20} would be quite reactive and unstable. However, experimental findings suggest that C_{20} is not as reactive as a pure biradical.¹⁰¹ It is likely that the global minimum structure would be one of the Jahn-Teller distorted structures or other structures such as bowl suggested in literature. Providing an answer to this question would require geometry optimization with κ -OOMP2 and this would be an interesting research direction to pursue in the future.

5 Summary

We have presented an unbiased analysis to determine whether fullerenes, C_{20} , C_{36} , and C_{60} , are strongly correlated. At the Hartree-Fock level, this was already done based on the existence of complex, generalized Hartree-Fock (cGHF) solutions in the work by Jiménez-Hoyos et al. As it is common to observe artificial symmetry at the HF level in innocent (i.e., not strongly correlated) systems, we analyzed these solutions beyond the HF level. This was achieved with three different probes.

First, we used the recently developed regularized orbital-optimized second-order Møller-Plesset perturbation theory (κ -OOMP2) to obtain landscapes of symmetry breaking parameters for spin operators \hat{S}^2 and \hat{S}_n and complex operator \hat{K} as a function of the regularization strength κ . The critical strength κ_c was then used to determine whether a given fullerene is strongly correlated. If κ_c is around 1.0, which is far stronger than the optimal κ we determined in our previous work, we concluded that the symmetry breaking at the HF level is artificial.

Second, we obtained the singlet-triplet gaps of these fullerenes and quantified strong correlation in them. A singlet-triplet gap measures an energy cost of unpairing an electron pair and this energy cost should be small if the system has strong biradicaloid character.

Lastly, we studied strong correlation within a minimal basis using two coupled-cluster (CC) methods along with various unregularized OOMP2 methods and κ -OOMP2. The two methods used in this work are restricted CC with singles and doubles (RCCSD) and CC valence-bond with singles and doubles (CCVB-SD). Based on our previous work,⁴⁰ it is well understood that there is a qualitative difference between RCCSD and CCVB-SD when strong correlation is present. This qualitative difference was probed with natural orbital occupation numbers (NOONs). NOONs from CCVB-SD were in general qualitatively consistent with NOONs from κ -OOMP2 for the systems we considered in this work. Based on these three independent probes, we reached the following conclusions.

C_{60} is *not strongly correlated* and the symmetry breaking present in its cGHF solution is *artificial* based on all three probes. The critical κ values for each symmetry breaking is in the range of artificial symmetry breaking. Its singlet-triplet gap is large in both experiments and computations. Furthermore, RCCSD and CCVB-SD show nearly identical behavior. Therefore, the molecule should be described as a closed shell molecule. This is not surprising due to the fact that it is electron paramagnetic resonance silent and found stable in experiments. This then contradicts with the conclusion drawn by Jiménez-Hoyos and co-workers.

On the other hand, C_{36} within the D_{6h} point group is strongly correlated. In particular, it is a singlet biradicaloid where unrestricted treatment in conjunction with Yamaguchi’s approximate projection can be used to obtain a qualitatively (and even quantitatively) correct answer. The cGHF solution found by Jiménez-Hoyos et al is likely an artifact due to the limited treatment of electron correlation: the complex and $\langle \hat{S}_n \rangle$ symmetry breakings are *artificial*. However, since breaking $\langle \hat{S}^2 \rangle$ symmetry was found to be *essential*, we conclude that this system is strongly correlated. The singlet-triplet gap of this molecule was found to be small and a qualitative difference between the NOONs of RCCSD and CCVB-SD was observed. All three probes indicate that the symmetry breaking in C_{36} is *essential* and C_{36} is strongly correlated.

Lastly, we applied the first probe to the smallest fullerene C_{20} . A total of five geometries

of C_{20} considered in this work all exhibit symmetry breaking. All of the Jahn-Teller distorted geometries (C_{2h} , D_{2h} , C_i , and D_{3h}) were found not to be strongly correlated and the underlying Hartree-Fock symmetry breaking is therefore *artificial*. On the other hand, the fully symmetric dodecahedral geometry (I_h) was found to be strongly correlated. In particular, it exhibits a near-zero singlet-triplet gap.

It is the central message of this paper that not every symmetry breaking in a HF solution indicates strong correlation. Many symmetry breakings in Hartree-Fock are simply due to its lack of dynamic correlation, which can be properly recovered by perturbation theory such as MP2. κ -OOMP2 emerges as a method that captures dynamic correlation, and attenuates all strong correlation. As a result, κ -OOMP2 removes artificial symmetry breaking in its reference determinant. However, essential symmetry breaking due to lack of static (or strong) correlation remains. The analyses we presented here can be used to probe strong correlation in numerous chemical systems especially when one is unsure about using single-reference methods.

6 Acknowledgement

We thank Dave Small for bringing our attention to this problem in the beginning, Eloy Ramos and Luke Bertels for stimulating discussions, and Evgeny Epifanovsky and Xintian Feng for useful discussions on efficient implementations. J.L. thanks Soojin Lee for consistent encouragement. This work was supported by the Director, Office of Science, Office of Basic Energy Sciences of the U.S. Department of Energy under contract No. DE-ACO2-05CH11231.

7 Appendix

7.1 Non-Collinearity Test of MP1 Wavefunctions

In order to perform the non-collinearity test on an MP1 wavefunction, one needs first-order corrections to $\langle \hat{S}_i \rangle$ and $\langle \hat{S}_i \hat{S}_j \rangle$ where $i, j \in \{x, y, z\}$. The first-order correction to $\langle \hat{O} \rangle$ for an operator \hat{O} is defined as follows:

$$\langle \hat{O} \rangle_1 = \langle \Psi_1 | \hat{O} | \Psi_0 \rangle + \langle \Psi_0 | \hat{O} | \Psi_1 \rangle. \quad (\text{A1})$$

This can be derived from the derivative with respect to λ of the first-order MP energy expression $E^{(1)}$ with a modified Hamiltonian, $\hat{H} + \lambda \hat{O}$. We enumerate the expectation value of each spin operator using this formula. For $\langle \hat{S}^2 \rangle$, one may use the following identity:

$$\hat{S}^2 = \hat{S}_z + \hat{S}_z^2 + \hat{S}_- \hat{S}_+, \quad (\text{A2})$$

where

$$\hat{S}_z = \frac{1}{2} \sum_p \left(\hat{a}_{p_\alpha}^\dagger \hat{a}_{p_\alpha} - \hat{a}_{p_\beta}^\dagger \hat{a}_{p_\beta} \right) \quad (\text{A3})$$

$$\hat{S}_+ = \hat{S}_x + i\hat{S}_y = \sum_p \hat{a}_{p_\alpha}^\dagger \hat{a}_{p_\beta} \quad (\text{A4})$$

$$\hat{S}_- = \hat{S}_x - i\hat{S}_y = \sum_p \hat{a}_{p_\beta}^\dagger \hat{a}_{p_\alpha} \quad (\text{A5})$$

One can evaluate $\langle \hat{S}_i \hat{S}_j \rangle$ for $i, j \in \{x, y\}$ using $\langle \hat{S}_i \hat{S}_j \rangle$ for $i, j \in \{+, -\}$. We choose to work with these ladder operators for simplicity.

With a cGHF reference, the zeroth order expectation values are as follows:^{45,46}

$$\langle \hat{S}_z \rangle_0 = \frac{1}{2} \sum_i (\langle i_\alpha | i_\alpha \rangle - \langle i_\beta | i_\beta \rangle) \quad (\text{A6})$$

$$\langle \hat{S}_+ \rangle_0 = \langle \hat{S}_- \rangle_0^* = \sum_i \langle i_\alpha | i_\beta \rangle \quad (\text{A7})$$

$$\begin{aligned} \langle \hat{S}_z^2 \rangle_0 &= \frac{1}{4} \sum_i (\langle i_\alpha | i_\alpha \rangle + \langle i_\beta | i_\beta \rangle) \\ &\quad + \frac{1}{4} \sum_{ij} \sum_{\sigma \in \{\alpha, \beta\}} (\langle i_\sigma | i_\sigma \rangle \langle j_\sigma | j_\sigma \rangle - \langle i_\sigma | j_\sigma \rangle \langle j_\sigma | i_\sigma \rangle) \\ &\quad + \frac{1}{4} \sum_{ij} (\langle i_\beta | j_\beta \rangle \langle j_\alpha | i_\alpha \rangle - \langle i_\alpha | i_\alpha \rangle \langle j_\beta | j_\beta \rangle + \text{h.c.}) \end{aligned} \quad (\text{A8})$$

$$\langle \hat{S}_- \hat{S}_+ \rangle_0 = \sum_i \langle i_\beta | i_\beta \rangle + \sum_{ij} (\langle i_\alpha | i_\beta \rangle \langle j_\beta | j_\alpha \rangle - \langle i_\beta | j_\alpha \rangle \langle j_\alpha | i_\beta \rangle) \quad (\text{A9})$$

$$\langle \hat{S}_+ \hat{S}_- \rangle_0 = \sum_i \langle i_\alpha | i_\alpha \rangle + \sum_{ij} (\langle i_\alpha | i_\beta \rangle \langle j_\beta | j_\alpha \rangle - \langle i_\beta | j_\alpha \rangle \langle j_\alpha | i_\beta \rangle) \quad (\text{A10})$$

$$\langle \hat{S}_- \hat{S}_- \rangle_0 = \langle \hat{S}_+ \hat{S}_+ \rangle_0^* = \sum_{ij} (\langle i_\beta | i_\alpha \rangle \langle j_\beta | j_\alpha \rangle - \langle j_\beta | i_\alpha \rangle \langle i_\beta | j_\alpha \rangle) \quad (\text{A11})$$

$$\begin{aligned} \langle \hat{S}_+ \hat{S}_z \rangle_0 = \langle \hat{S}_z \hat{S}_- \rangle_0^* &= -\frac{1}{2} \sum_i \langle i_\alpha | i_\beta \rangle + \frac{1}{2} \sum_{ij} (\langle i_\alpha | i_\beta \rangle \langle j_\alpha | j_\alpha \rangle - \langle j_\alpha | i_\beta \rangle \langle i_\alpha | j_\alpha \rangle) \\ &\quad - \frac{1}{2} \sum_{ij} (\langle i_\alpha | i_\beta \rangle \langle j_\beta | j_\beta \rangle - \langle i_\beta | j_\beta \rangle \langle j_\alpha | i_\beta \rangle) \end{aligned} \quad (\text{A12})$$

$$\begin{aligned} \langle \hat{S}_- \hat{S}_z \rangle_0 = \langle \hat{S}_z \hat{S}_+ \rangle_0^* &= \frac{1}{2} \sum_i \langle i_\beta | i_\alpha \rangle + \frac{1}{2} \sum_{ij} (\langle i_\beta | i_\alpha \rangle \langle j_\alpha | j_\alpha \rangle - \langle i_\alpha | j_\alpha \rangle \langle j_\beta | i_\alpha \rangle) \\ &\quad - \frac{1}{2} \sum_{ij} (\langle i_\beta | i_\alpha \rangle \langle j_\beta | j_\beta \rangle - \langle i_\beta | j_\beta \rangle \langle j_\beta | i_\alpha \rangle) \end{aligned} \quad (\text{A13})$$

where we used the fact that each orbital is of the spinor form in Eq. (6) and we define

$$\langle p_{\sigma_1} | q_{\sigma_2} \rangle = \int_{\mathbf{r}} (\phi_p^{\sigma_1}(\mathbf{r}))^* \phi_q^{\sigma_2}(\mathbf{r}). \quad (\text{A14})$$

We note that there is no spin integration in Eq. (A14). These are used to compute the covariance matrix $A_{ij} = \langle \hat{S}_i \hat{S}_j \rangle - \langle \hat{S}_i \rangle \langle \hat{S}_j \rangle$. As noted before, the eigenspectrum of \mathbf{A} determines whether the GHF wavefunction is genuinely non-collinear. The wavefunction is collinear if

and only if there is a zero eigenmode.

Similarly, the first-order corrections to these expectation values can be obtained from

$$\langle \hat{O} \rangle_1 = \frac{1}{4} \sum_{ijab} (t_{ij}^{ab})^* \langle \Psi_{ij}^{ab} | \hat{O} | \Psi_0 \rangle + \frac{1}{4} \sum_{ijab} \langle \Psi_0 | \hat{O} | \Psi_{ij}^{ab} \rangle t_{ij}^{ab} \quad (\text{A15})$$

This can be easily computed as follows:

$$\langle \hat{S}_z \rangle_1 = \langle \hat{S}_+ \rangle_1 = \langle \hat{S}_- \rangle_1 = 0 \quad (\text{A16})$$

$$\begin{aligned} \langle \hat{S}_z^2 \rangle_1 &= \frac{1}{4} \sum_{\substack{i<j \\ a<b}} (t_{ij}^{ab})^* \sum_{\sigma \in \{\alpha, \beta\}} (2\langle a_\sigma | i_\sigma \rangle \langle b_\sigma | j_\sigma \rangle - 2\langle a_\sigma | j_\sigma \rangle \langle b_\sigma | i_\sigma \rangle) \\ &+ \frac{1}{4} \sum_{\substack{i<j \\ a<b}} (t_{ij}^{ab})^* (-2\langle a_\alpha | i_\alpha \rangle \langle b_\beta | j_\beta \rangle + 2\langle a_\beta | j_\beta \rangle \langle b_\alpha | i_\alpha \rangle \\ &- 2\langle a_\beta | i_\beta \rangle \langle b_\alpha | j_\alpha \rangle + 2\langle a_\alpha | j_\alpha \rangle \langle b_\beta | i_\beta \rangle) + \text{h.c.} \end{aligned} \quad (\text{A17})$$

$$\begin{aligned} \langle \hat{S}_- \hat{S}_+ \rangle_1 = \langle \hat{S}_+ \hat{S}_- \rangle_1 &= \sum_{\substack{i<j \\ a<b}} (t_{ij}^{ab})^* (\langle a_\beta | i_\alpha \rangle \langle b_\alpha | j_\beta \rangle - \langle a_\alpha | j_\beta \rangle \langle b_\beta | i_\alpha \rangle \\ &+ \langle a_\alpha | i_\beta \rangle \langle b_\beta | j_\alpha \rangle - \langle a_\beta | j_\alpha \rangle \langle b_\alpha | i_\beta \rangle) + \text{h.c.} \end{aligned} \quad (\text{A18})$$

$$\begin{aligned} \langle \hat{S}_- \hat{S}_- \rangle_1 = \langle \hat{S}_+ \hat{S}_+ \rangle_1^* &= \sum_{\substack{i<j \\ a<b}} (t_{ij}^{ab})^* (2\langle a_\beta | i_\alpha \rangle \langle b_\beta | j_\alpha \rangle - 2\langle a_\beta | j_\alpha \rangle \langle b_\beta | i_\alpha \rangle) \\ &+ \sum_{\substack{i<j \\ a<b}} (t_{ij}^{ab}) (2\langle i_\beta | a_\alpha \rangle \langle j_\beta | b_\alpha \rangle - 2\langle j_\beta | a_\alpha \rangle \langle i_\beta | b_\alpha \rangle) \end{aligned} \quad (\text{A19})$$

$$\begin{aligned}
\langle \hat{S}_+ \hat{S}_z \rangle_1 = \langle \hat{S}_z \hat{S}_- \rangle_1^* &= \frac{1}{2} \sum_{\substack{i < j \\ a < b}} (t_{ij}^{ab})^* (\langle a_\alpha | i_\beta \rangle \langle b_\alpha | j_\alpha \rangle - \langle a_\alpha | j_\alpha \rangle \langle b_\alpha | i_\beta \rangle) \\
&+ \langle a_\alpha | i_\alpha \rangle \langle b_\alpha | j_\beta \rangle - \langle a_\alpha | j_\beta \rangle \langle b_\alpha | i_\alpha \rangle - \langle a_\alpha | i_\beta \rangle \langle b_\beta | j_\beta \rangle \\
&+ \langle a_\beta | j_\beta \rangle \langle b_\alpha | i_\beta \rangle - \langle a_\beta | i_\beta \rangle \langle b_\alpha | j_\beta \rangle + \langle a_\alpha | j_\beta \rangle \langle b_\beta | i_\beta \rangle) \\
&+ \frac{1}{2} \sum_{\substack{i < j \\ a < b}} t_{ij}^{ab} (\langle i_\alpha | a_\alpha \rangle \langle j_\alpha | b_\beta \rangle - \langle j_\alpha | a_\beta \rangle \langle i_\alpha | b_\alpha \rangle) \\
&+ \langle i_\alpha | a_\beta \rangle \langle j_\alpha | b_\alpha \rangle - \langle j_\alpha | a_\alpha \rangle \langle i_\alpha | b_\beta \rangle - \langle i_\beta | a_\beta \rangle \langle j_\alpha | b_\beta \rangle \\
&+ \langle j_\alpha | a_\beta \rangle \langle i_\beta | b_\beta \rangle - \langle i_\alpha | a_\beta \rangle \langle j_\beta | b_\beta \rangle + \langle j_\beta | a_\alpha \rangle \langle i_\alpha | b_\beta \rangle) \quad (A20)
\end{aligned}$$

$$\begin{aligned}
\langle \hat{S}_- \hat{S}_z \rangle_1 = \langle \hat{S}_z \hat{S}_+ \rangle_1^* &= \frac{1}{2} \sum_{\substack{i < j \\ a < b}} (t_{ij}^{ab})^* (\langle a_\beta | i_\alpha \rangle \langle b_\alpha | j_\alpha \rangle - \langle a_\alpha | j_\alpha \rangle \langle b_\beta | i_\alpha \rangle) \\
&+ \langle a_\alpha | i_\alpha \rangle \langle b_\beta | j_\alpha \rangle - \langle a_\beta | j_\alpha \rangle \langle b_\alpha | i_\alpha \rangle - \langle a_\beta | i_\alpha \rangle \langle b_\beta | j_\beta \rangle \\
&+ \langle a_\beta | j_\beta \rangle \langle b_\beta | i_\alpha \rangle - \langle a_\beta | i_\beta \rangle \langle b_\beta | j_\alpha \rangle + \langle a_\beta | j_\alpha \rangle \langle b_\beta | i_\beta \rangle) \\
&+ \frac{1}{2} \sum_{\substack{i < j \\ a < b}} t_{ij}^{ab} (\langle i_\alpha | a_\alpha \rangle \langle j_\beta | b_\beta \rangle - \langle j_\beta | a_\alpha \rangle \langle i_\alpha | b_\alpha \rangle) \\
&+ \langle i_\beta | a_\alpha \rangle \langle j_\alpha | b_\alpha \rangle - \langle j_\alpha | a_\alpha \rangle \langle i_\beta | b_\alpha \rangle - \langle i_\beta | a_\beta \rangle \langle j_\beta | b_\alpha \rangle \\
&+ \langle j_\beta | a_\alpha \rangle \langle i_\beta | b_\beta \rangle - \langle i_\beta | a_\alpha \rangle \langle j_\beta | b_\beta \rangle + \langle j_\beta | a_\beta \rangle \langle i_\beta | b_\alpha \rangle) \quad (A21)
\end{aligned}$$

7.2 Complex Generalized HF

The variation in the energy expression reads

$$\delta E = \sum_{ia} (-h_{ai} \delta \Theta_{ia} - h_{ia} \delta \Theta_{ia}^*) - \frac{1}{2} \sum_{ija} (\langle ij || aj \rangle \delta \Theta_{ia}^* + \langle ij || ia \rangle \delta \Theta_{ja}^* + \langle aj || ij \rangle \delta \Theta_{ia} + \langle ia || ij \rangle \delta \Theta_{ja})$$

where $\delta \Theta_{ia}$ is an infinitesimal orbital rotation. This energy variation can be used to compute orbital gradient and similarly orbital hessian.

7.2.1 Orbital Gradient

We compute the gradient of E with respect to the real and imaginary part of Θ ,

$$\frac{\partial E}{\partial \text{Re}(\Theta_{ia})} = -[h_{ai} + J_{ai} - K_{ai}] + \text{h.c.} = -h_{ai} - \sum_k \langle ak || ik \rangle - h_{ia} - \sum_k \langle ik || ak \rangle$$

$$\frac{\partial E}{\partial i\text{Im}(\Theta_{ia})} = -[h_{ai} + J_{ai} - K_{ai}] - \text{h.c.} = -h_{ai} - \sum_k \langle ak || ik \rangle + h_{ia} + \sum_k \langle ik || ak \rangle$$

7.2.2 Orbital Hessian

The variation of orbital gradient reads

$$\begin{aligned} \delta \frac{\partial E}{\partial \text{Re}(\Theta_{ia})} &= \sum_j (-h_{ji} \delta \Theta_{ja}^* + h_{ab} \delta \Theta_{bi}^*) + \sum_k \left(-\sum_j \delta \Theta_{aj}^* \langle jk || ik \rangle + \sum_b \delta \Theta_{bi}^* \langle ak || bk \rangle \right) \\ &\quad + \sum_{kb} \delta \Theta_{bk}^* \langle ak || ib \rangle + \sum_{kb} \delta \Theta_{bk} \langle ab || ik \rangle + \text{h.c.} \end{aligned} \quad (\text{A22})$$

and

$$\begin{aligned} \delta \frac{\partial E}{\partial i\text{Im}(\Theta_{ia})} &= \sum_j (-h_{ji} \delta \Theta_{ja}^* + h_{ab} \delta \Theta_{bi}^*) + \sum_k \left(-\sum_j \delta \Theta_{aj}^* \langle jk || ik \rangle + \sum_b \delta \Theta_{bi}^* \langle ak || bk \rangle \right) \\ &\quad + \sum_{kb} \delta \Theta_{bk}^* \langle ak || ib \rangle + \sum_{kb} \delta \Theta_{bk} \langle ab || ik \rangle - \text{h.c.} \end{aligned} \quad (\text{A23})$$

These are then used to obtain orbital hessian:

$$\frac{\partial^2 E}{\partial \text{Re}(\Theta_{ia}) \partial \text{Re}(\Theta_{jb})} = \left[-\delta_{ab} \left(h_{ji} + \sum_k \langle jk || ik \rangle \right) + \delta_{ij} \left(h_{ab} + \sum_k \langle ak || bk \rangle \right) + \langle aj || ib \rangle + \langle ab || ij \rangle \right] + \text{h.c.} \quad (\text{A24})$$

$$\begin{aligned} \frac{\partial^2 E}{\partial i\text{Im}(\Theta_{ia})\partial i\text{Im}(\Theta_{jb})} &= \left[\delta_{ab} \left(h_{ji} + \sum_k \langle jk||ik \rangle \right) - \delta_{ij} \left(h_{ab} + \sum_k \langle ak||bk \rangle \right) - \langle aj||ib \rangle + \langle ab||ij \rangle \right] + h.c. \\ &= -\frac{\partial^2 E}{\partial \text{Im}(\Theta_{ia})\partial \text{Im}(\Theta_{jb})} \end{aligned} \quad (\text{A25})$$

$$\frac{\partial^2 E}{\partial \text{Im}(\Theta_{ia})\partial \text{Re}(\Theta_{jb})} = i[-\langle aj||ib \rangle + \langle ab||ij \rangle - h.c.] \quad (\text{A26})$$

$$\frac{\partial^2 E}{\partial \text{Re}(\Theta_{ia})\partial \text{Im}(\Theta_{jb})} = -i[-\langle aj||ib \rangle + \langle ab||ij \rangle - h.c.] \quad (\text{A27})$$

References

- (1) Pulay, P.; Hamilton, T. P. *J. Chem. Phys.* **1988**, *88*, 4926–4933.
- (2) Bofill, J. M.; Pulay, P. *J. Chem. Phys.* **1989**, *90*, 3637–3646.
- (3) Coulson, C.; Fischer, I. *Philos. Mag.* **1949**, *40*, 386–393.
- (4) Jackels, C. F.; Davidson, E. R. *J. Chem. Phys.* **1976**, *64*, 2908–2917.
- (5) Davidson, E. R.; Borden, W. T. *J. Phys. Chem.* **1983**, *87*, 4783–4790.
- (6) Andrews, J. S.; Jayatilaka, D.; Bone, R. G.; Handy, N. C.; Amos, R. D. *Chem. Phys. Lett.* **1991**, *183*, 423–431.
- (7) Ayala, P. Y.; Schlegel, H. B. *J. Chem. Phys.* **1998**, *108*, 7560.
- (8) McLean, A. D.; Lengsfeld, B. H.; Pacansky, J.; Ellinger, Y. *J. Chem. Phys.* **1985**, *83*, 3567–3576.
- (9) Sherrill, C.; Lee, M. S.; Head-Gordon, M. *Chem. Phys. Lett.* **1999**, *302*, 425–430.

- (10) Crawford, T. D.; Stanton, J. F. *J. Chem. Phys.* **2000**, *112*, 7873.
- (11) Paldus, J.; Thiamová, G. *J. Math. Chem.* **2007**, *44*, 88–120.
- (12) Small, D.; Zaitsev, V.; Jung, Y.; Rosokha, S. V.; Head-Gordon, M.; Kochi, J. K. *J. Am. Chem. Soc.* **2004**, *126*, 13850–13858, PMID: 15493946.
- (13) Small, D.; Rosokha, S. V.; Kochi, J. K.; Head-Gordon, M. *J. Phys. Chem. A* **2005**, *109*, 11261–11267, PMID: 16331910.
- (14) Lochan, R. C.; Head-Gordon, M. *J. Chem. Phys.* **2007**, *126*, 164101.
- (15) Lykos, P.; Pratt, G. W. *Rev. Mod. Phys.* **1963**, *35*, 496–501.
- (16) Farnell, L.; Pople, J. A.; Radom, L. *J. Phys. Chem.* **1983**, *87*, 79–82.
- (17) Nobes, R. H.; Pople, J. A.; Radom, L.; Handy, N. C.; Knowles, P. J. *Chem. Phys. Lett.* **1987**, *138*, 481–485.
- (18) Gill, P. M. W.; Pople, J. A.; Radom, L.; Nobes, R. H. *J. Chem. Phys.* **1988**, *89*, 7307–7314.
- (19) Jensen, F. *Chem. Phys. Lett.* **1990**, *169*, 519–528.
- (20) Yamanaka, S.; Okumura, M.; Nakano, M.; Yamaguchi, K. *J. Mol. Struct.* **1994**, *310*, 205–218.
- (21) Meyer, W. *J. Chem. Phys.* **1976**, *64*, 2901–2907.
- (22) Shavitt, I.; Rosenberg, B. J.; Palalikit, S. *Int. J. Quantum Chem.* **1976**, *10*, 33–46.
- (23) Dykstra, C. E. *Chem. Phys. Lett.* **1977**, *45*, 466–469.
- (24) Handy, N. C.; Pople, J. A.; Head-Gordon, M.; Raghavachari, K.; Trucks, G. W. *Chem. Phys. Lett.* **1989**, *164*, 185–192.

- (25) Brueckner, K. A. *Phys. Rev.* **1954**, *96*, 508–516.
- (26) Nesbet, R. K. *Phys. Rev.* **1958**, *109*, 1632–1638.
- (27) Sherrill, C. D.; Krylov, A. I.; Byrd, E. F. C.; Head-Gordon, M. *J. Chem. Phys.* **1998**, *109*, 4171–4181.
- (28) Krylov, A. I.; Sherrill, C. D.; Byrd, E. F. C.; Head-Gordon, M. *J. Chem. Phys.* **1998**, *109*, 10669.
- (29) Stück, D.; Baker, T. A.; Zimmerman, P.; Kurlancheek, W.; Head-Gordon, M. *J. Chem. Phys.* **2011**, *135*, 194306.
- (30) Kurlancheek, W.; Lochan, R.; Lawler, K.; Head-Gordon, M. *J. Chem. Phys.* **2012**, *136*, 054113.
- (31) Neese, F.; Schwabe, T.; Kossmann, S.; Schirmer, B.; Grimme, S. *J. Chem. Theory Comput.* **2009**, *5*, 3060–3073.
- (32) Kossmann, S.; Neese, F. *J. Phys. Chem. A* **2010**, *114*, 11768–11781.
- (33) Stück, D.; Head-Gordon, M. *J. Chem. Phys.* **2013**, *139*, 244109.
- (34) Razban, R. M.; Stück, D.; Head-Gordon, M. *Mol. Phys.* **2017**, *115*, 2102–2109.
- (35) Lee, J.; Head-Gordon, M. *J. Chem. Theory Comput.* **2018**, *14*, 5203–5219.
- (36) Fowler, P. W.; Manolopoulos, D. E. *An Atlas of Fullerenes (Dover Books on Chemistry)*; Dover Publications, 2007.
- (37) Prinzbach, H.; Weiler, A.; Landenberger, P.; Wahl, F.; Wörth, J.; Scott, L. T.; Gelmont, M.; Olevano, D.; v. Issendorff, B. *Nature* **2000**, *407*, 60–63.
- (38) Jiménez-Hoyos, C. A.; Rodríguez-Guzmán, R.; Scuseria, G. E. *J. Phys. Chem. A* **2014**, *118*, 9925–40.

- (39) Small, D. W.; Head-Gordon, M. *J. Chem. Phys.* **2012**, *137*, 114103.
- (40) Lee, J.; Small, D. W.; Epifanovsky, E.; Head-Gordon, M. *J. Chem. Theory Comput.* **2017**, *13*, 602–615.
- (41) Fukutome, H. *Int. J. Quantum Chem.* **1981**, *20*, 955–1065.
- (42) Stuber, J. L.; Paldus, J. In *Fundamental World of Quantum Chemistry: A Tribute to the Memory of Per-Olov Ludin*; Brändas, E. J., Kryachko, E. S., Eds.; Springer, 2003; Vol. 1; pp 67–139.
- (43) Yamaki, D.; Shigeta, Y.; Yamanaka, S.; Nagao, H.; Yamaguchi, K. *Int. J. Quantum Chem.* **2000**, *80*, 701–707.
- (44) Jiménez-Hoyos, C. A.; Henderson, T. M.; Scuseria, G. E. *J. Chem. Theory Comput.* **2011**, *7*, 2667–2674.
- (45) Small, D. W.; Sundstrom, E. J.; Head-Gordon, M. *J. Chem. Phys.* **2015**, *142*, 094112.
- (46) Cassam-Chenaï, P. *Theor. Chem. Acc.* **2015**, *134*, 125.
- (47) Feyereisen, M.; Fitzgerald, G.; Komornicki, A. *Chem. Phys. Lett.* **1993**, *208*, 359–363.
- (48) Bernholdt, D. E.; Harrison, R. J. *Chem. Phys. Lett.* **1996**, *250*, 477–484.
- (49) Small, D. W.; Sundstrom, E. J.; Head-Gordon, M. *J. Chem. Phys.* **2015**, *142*, 024104.
- (50) Small, D. W.; Head-Gordon, M. *J. Chem. Phys.* **2009**, *130*, 084103.
- (51) Small, D. W.; Head-Gordon, M. *Phys. Chem. Chem. Phys.* **2011**, *13*, 19285–97.
- (52) Small, D. W.; Lawler, K. V.; Head-Gordon, M. *J. Chem. Theory Comput.* **2014**, *10*, 2027–2040.
- (53) Small, D. W.; Head-Gordon, M. *J. Chem. Phys.* **2017**, *147*, 024107.

- (54) Small, D. W.; Head-Gordon, M. *J. Chem. Phys.* **2018**, *149*, 144103.
- (55) Lee, J.; Small, D. W.; Head-Gordon, M. *arXiv:1808.06743*.
- (56) Abe, M. *Chem. Rev.* **2013**, *113*, 7011–7088.
- (57) Head-Gordon, M. *Chem. Phys. Lett.* **2003**, *372*, 508–511.
- (58) Shao, Y.; Gan, Z.; Epifanovsky, E.; Gilbert, A. T.; Wormit, M.; Kussmann, J.; Lange, A. W.; Behn, A.; Deng, J.; Feng, X.; Ghosh, D.; Goldey, M.; Horn, P. R.; Jacobson, L. D.; Kaliman, I.; Khaliullin, R. Z.; Kuś, T.; Landau, A.; Liu, J.; Proynov, E. I.; Rhee, Y. M.; Richard, R. M.; Rohrdanz, M. A.; Steele, R. P.; Sundstrom, E. J.; Woodcock, H. L.; Zimmerman, P. M.; Zuev, D.; Albrecht, B.; Alguire, E.; Austin, B.; Beran, G. J.; Bernard, Y. A.; Berquist, E.; Brandhorst, K.; Bravaya, K. B.; Brown, S. T.; Casanova, D.; Chang, C. M.; Chen, Y.; Chien, S. H.; Closser, K. D.; Crittenden, D. L.; Diedenhofen, M.; Distasio, R. A.; Do, H.; Dutoi, A. D.; Edgar, R. G.; Fatehi, S.; Fusti-Molnar, L.; Ghysels, A.; Golubeva-Zadorozhnaya, A.; Gomes, J.; Hanson-Heine, M. W.; Harbach, P. H.; Hauser, A. W.; Hohenstein, E. G.; Holden, Z. C.; Jagau, T. C.; Ji, H.; Kaduk, B.; Khistyayev, K.; Kim, J.; Kim, J.; King, R. A.; Klunzinger, P.; Kosenkov, D.; Kowalczyk, T.; Krauter, C. M.; Lao, K. U.; Laurent, A. D.; Lawler, K. V.; Levchenko, S. V.; Lin, C. Y.; Liu, F.; Livshits, E.; Lochan, R. C.; Luenser, A.; Manohar, P.; Manzer, S. F.; Mao, S. P.; Mardirossian, N.; Marenich, A. V.; Maurer, S. A.; Mayhall, N. J.; Neuscamman, E.; Oana, C. M.; Olivares-Amaya, R.; Oneill, D. P.; Parkhill, J. A.; Perrine, T. M.; Peverati, R.; Prociuk, A.; Rehn, D. R.; Rosta, E.; Russ, N. J.; Sharada, S. M.; Sharma, S.; Small, D. W.; Sodt, A.; Stein, T.; Stück, D.; Su, Y. C.; Thom, A. J.; Tsuchimochi, T.; Vanovschi, V.; Vogt, L.; Vydrov, O.; Wang, T.; Watson, M. A.; Wenzel, J.; White, A.; Williams, C. F.; Yang, J.; Yeganeh, S.; Yost, S. R.; You, Z. Q.; Zhang, I. Y.; Zhang, X.; Zhao, Y.; Brooks, B. R.; Chan, G. K.; Chipman, D. M.; Cramer, C. J.; Goddard, W. A.; Gordon, M. S.; Hehre, W. J.; Klamt, A.; Schaefer, H. F.; Schmidt, M. W.; Sherrill, C. D.; Truh-

- lar, D. G.; Warshel, A.; Xu, X.; Aspuru-Guzik, A.; Baer, R.; Bell, A. T.; Besley, N. A.; Chai, J. D.; Dreuw, A.; Dunietz, B. D.; Furlani, T. R.; Gwaltney, S. R.; Hsu, C. P.; Jung, Y.; Kong, J.; Lambrecht, D. S.; Liang, W.; Ochsenfeld, C.; Rassolov, V. A.; Slipchenko, L. V.; Subotnik, J. E.; Van Voorhis, T.; Herbert, J. M.; Krylov, A. I.; Gill, P. M.; Head-Gordon, M. *Mol. Phys.* **2015**, *113*, 184–215.
- (59) Hunter, J. D. *Comput. Sci. Eng.* **2007**, *9*, 90–95.
- (60) Chemcraft. <https://www.chemcraftprog.com>, Accessed: 2017-10-31.
- (61) Paul, P.; Kim, K.-C.; Sun, D.; Boyd, P. D. W.; Reed, C. A. *J. Am. Chem. Soc.* **2002**, *124*, 4394–4401.
- (62) Tomita, S.; Andersen, J.; Hansen, K.; Hvelplund, P. *Chem. Phys. Lett.* **2003**, *382*, 120–125.
- (63) Hehre, W. J.; Stewart, R. F.; Pople, J. A. *J. Chem. Phys.* **1969**, *51*, 2657–2664.
- (64) Dunning, T. H. *J. Chem. Phys.* **1989**, *90*, 1007–1023.
- (65) Sassara, A.; Zerza, G.; Chergui, M. *Chem. Phys. Lett.* **1996**, *261*, 213–220.
- (66) Weigend, F.; Köhn, A.; Hättig, C. *J. Chem. Phys.* **2002**, *116*, 3175–3183.
- (67) Varganov, S. A.; Avramov, P. V.; Ovchinnikov, S. G.; Gordon, M. S. *Chem. Phys. Lett.* **2002**, *362*, 380–386.
- (68) Piskoti, C.; Yarger, J.; Zetl, A. *Nature* **1998**, *393*, 771–774.
- (69) Fowler, P.; Heine, T.; Rogers, K.; Sandall, J.; Seifert, G.; Zerbetto, F. *Chem. Phys. Lett.* **1999**, *300*, 369–378.
- (70) Fowler, P. W.; Mitchell, D.; Zerbetto, F. *Journal of the American Chemical Society* **1999**, *121*, 3218–3219.

- (71) Jagadeesh, M. N.; Chandrasekhar, J. *Chem. Phys. Lett.* **1999**, *305*, 298–302.
- (72) Ito, A.; Monobe, T.; Yoshii, T.; Tanaka, K. *Chem. Phys. Lett.* **2000**, *328*, 32–38.
- (73) Slanina, Z.; Uhlík, F.; Zhao, X.; Ōsawa, E. *J. Chem. Phys.* **2000**, *113*, 4933.
- (74) Yuan, L.-F.; Yang, J.; Deng, K.; Zhu, Q.-S. *J. Phys. Chem. A* **2000**, *104*, 6666–6671.
- (75) Paulus, B. *Phys. Chem. Chem. Phys.* **2003**, *5*, 3364.
- (76) Becke, A. D. *Phys. Rev. A* **1988**, *38*, 3098–3100.
- (77) Lee, C.; Yang, W.; Parr, R. G. *Phys. Rev. B* **1988**, *37*, 785–789.
- (78) Hariharan, P. C.; Pople, J. A. *Theor. Chim. Acta.* **1973**, *28*, 213–222.
- (79) Hehre, W. J.; Ditchfield, R.; Pople, J. A. *J. Chem. Phys.* **1972**, *56*, 2257–2261.
- (80) Grimme, S. *J. Chem. Phys.* **2003**, *118*, 9095–9102.
- (81) Jung, Y.; Lochan, R. C.; Dutoi, A. D.; Head-Gordon, M. *J. Chem. Phys.* **2004**, *121*, 9793–9802.
- (82) Yamaguchi, K.; Jensen, F.; Dorigo, A.; Houk, K. N. *Chem. Phys. Lett.* **1988**, *149*, 537–542.
- (83) Schwerdtfeger, P.; Wirz, L. N.; Avery, J. *WIREs: Comput. Mol. Sci.* **2015**, *5*, 96–145.
- (84) Parasuk, V.; Almlöf, J. *Chem. Phys. Lett.* **1991**, *184*, 187–190.
- (85) Feyereisen, M.; Gutowski, M.; Simons, J.; Almlöf, J. *J. Chem. Phys.* **1992**, *96*, 2926–2932.
- (86) Raghavachari, K.; Strout, D.; Odom, G.; Scuseria, G.; Pople, J.; Johnson, B.; Gill, P. *Chem. Phys. Lett.* **1993**, *214*, 357–361.

- (87) von Helden, G.; Hsu, M.; Gotts, N.; Kemper, P.; Bowers, M. *Chem. Phys. Lett.* **1993**, *204*, 15–22.
- (88) Bylaska, E. J.; Taylor, P. R.; Kawai, R.; Weare, J. H. *J. Phys. Chem.* **1996**, *100*, 6966–6972.
- (89) Martin, J. M.; El-Yazal, J.; François, J.-P. *Chem. Phys. Lett.* **1996**, *248*, 345–352.
- (90) Jones, R. O.; Seifert, G. *Phys. Rev. Lett.* **1997**, *79*, 443–446.
- (91) Kietzmann, H.; Rochow, R.; Ganteför, G.; Eberhardt, W.; Vietze, K.; Seifert, G.; Fowler, P. W. *Phys. Rev. Lett.* **1998**, *81*, 5378–5381.
- (92) Sokolova, S.; Lüchow, A.; Anderson, J. B. *Chem. Phys. Lett.* **2000**, *323*, 229–233.
- (93) Grimme, S.; Mück-Lichtenfeld, C. *ChemPhysChem* **2002**, *3*, 207–209.
- (94) Lu, J.; Re, S.; Choe, Y.-k.; Nagase, S.; Zhou, Y.; Han, R.; Peng, L.; Zhang, X.; Zhao, X. *Phys. Rev. B* **2003**, *67*, 125415.
- (95) An, W.; Gao, Y.; Bulusu, S.; Zeng, X. C. *J. Chem. Phys.* **2005**, *122*, 204109.
- (96) Jin, Y.; Perera, A.; Lotrich, V. F.; Bartlett, R. J. *Chem. Phys. Lett.* **2015**, *629*, 76–80.
- (97) Manna, D.; Martin, J. M. L. *J. Phys. Chem. A* **2016**, *120*, 153–160.
- (98) Adams, G. B.; Sankey, O. F.; Page, J. B.; O’Keeffe, M. *Chem. Phys.* **1993**, *176*, 61–66.
- (99) Krylov, A. I. *Chem. Phys. Lett.* **2001**, *338*, 375–384.
- (100) Fan, M.-F.; Lin, Z.; Yang, S. *J. Mol. Struct-THEOCHEM* **1995**, *337*, 231–240.
- (101) Prinzbach, H.; Wahl, F.; Weiler, A.; Landenberger, P.; Wörth, J.; Scott, L. T.; Gelmont, M.; Olevano, D.; Sommer, F.; von Issendorff, B. *Chem.-Eur. J.* **2006**, *12*, 6268–6280.